Theoretical and Experimental Study to Improve Antenna Performance Using a Resonant Choke Structure

by

Steven Petten

A thesis
presented to the University of Waterloo
in fulfillment of the
thesis requirement for the degree of
Master of Applied Science
in
Electrical and Computer Engineering

Waterloo, Ontario, Canada, 2014

I hereby declare that I am the sole author of this thesis. This is a true copy of the thesis, including any required final revisions, as accepted by my examiners.

I understand that my thesis may be made electronically available to the public.

Abstract

Every antenna requires a feed network to supply its RF energy. In the case of a simple dipole antenna, this could be a coaxial cable with a tuning element and matching balun. For mostly omnidirectional antennas, currents can easily couple to metallic surfaces inside an antenna's near field that includes the outer conductor of the coaxial feed line. These outer conductor currents can radiate into the far field to skew overall antenna radiation patterns. Other parameters such as VSWR may also be significantly affected. Electromagnetic field absorbers placed on the coaxial waveguide pose other problems where multiple RF carriers exist and non-linear dielectric materials can cause issues. Coil structures can also lead to radiation problems. This leads towards a metallic resonating choke solution, which will allow the antenna to radiate without affecting performance.

The primary goal of this research is to integrate a metallic resonant choke structure that will prevent currents from travelling down the feed line outer conductor. In this work, an in-depth analysis is performed on each antenna component. This includes the feed network elements (waveguide coaxial line, tuning element, matching balun) and the radiator (dipole arms, resonant choke, outer feed). Each element is analyzed and designed to allow the manufactured antenna to have similar performance to its ideal center-fed counterpart for a tuned frequency band.

To predict the performance of the manufactured antenna, several simulation models are constructed. To model the radiator and resonant choke structure, a Method of Moments code is written with Matlab. These results are compared with HFSS and measurements with good correlation. Specifically, the axisymmetric MoM code uses a KVL approach to integrate the internal choke structure that works well to reduce simulation time to a fraction of that taken by FEM solvers. To design the feed components, a combination of circuit models and HFSS allows for quick design with accurate results when compared with measured values. This systems design approach has the flexibility to add complexity to improve accuracy where needed.

Acknowledgements

I would first like to thank WADE Antenna for engaging the University of Waterloo in their research project. Their support was much appreciated throughout the duration of the project's preliminary design. I would also like to thank Mitacs for building the relationship between the University of Waterloo and WADE Antenna. To my wife Talar, I thank you for your continued patience to allow me to complete this research. Finally, I wish to kindly thank my research supervisor Professor Safieddin Safavi-Naeini for all of his guidance and discussions.

This is dedicated to my loving wife, Talar.

Table of Contents

List of Figures

Nomenclature

ADS	Advanced Design System
AUT	Antenna Under Test
DFM	Design For Manufacturing
FEM	Finite Element Method
HFSS	High Frequency Structural Simulator
LE	Lumped Element
MMM	Mode Matching Method
MoM	Method of Moments
PEC	Perfect Electrical Conductor
PIM	Passive Intermodulation
RF	Radio Frequency
UHF	Ultra High Frequency
VHF	Very High Frequency
VSWR	Voltage Standing Wave Ratio

Chapter 1

Introduction

Thin wire dipole antennas have been covered in nearly every standard antenna textbook and can be considered one of the most widely used antennas. In practical applications, dipoles are used in low and high power communication systems [7], but also could be used for special purposes such as in radar [9]. There are very few design parameters which makes them ideal candidates for easy design, manufacturing, and installation.

It is clear that every radiator element requires a feed network. In antenna simulation, the feed network is typically ignored, which can cause a problem when the manufactured antenna is measured [21, 30]. The feed network ranges in complexity depending on the system application. In the case of a cylindrical dipole antenna, there are only two main ways to place the feed network to minimize the effect of disturbing the far field radiation patterns. That is, perpendicular or parallel to the radiator arms. In the parallel configuration, the feed coaxial cable passes through the center of the hollow radiator cylinders and allows for the dipole to be easily mounted horizontally or vertically. It also allows for the dipole antennas to become stackable as shown in figure 1.1. In a standard installation, a vertical mounting structure is generally preferred; however, this comes at the consequence of disturbing antenna performance.

Figure 1.1: Dipole Antennas in Stacked or Array Form

Passing a feed line through the center of the radiator allows currents to be coupled by the radiated near field from the dipole arms. This, in turn, allows the feed line to radiate

energy which significantly decreases the performance. In the general case, the feed could also be considered a scatterer that can also negatively affect antenna performance [30]. This research will review methods to prevent currents from forming onto the feed coaxial cable line using several different techniques.

1.1 Scope

Whether a single dipole, stacked set of dipoles, or a dipole array is being designed, coupled near field currents are of significant importance and must either be designed to act positively on the performance of the antenna or be attenuated. Without intervention, the currents coupled to geometry around a dipole can have negative effects on its performance. This has been proven in simulation and in measured results [30].

The goal of this research is to provide means to understand, design, manufacture, assemble, test, and tune a new type of dipole antenna that eliminates currents when configured with a feed coax cable entering either end. This will be implemented in terms of a current choking structure that resonates with the antenna radiator instead of simply adding an impedance or inductive step. It also removes the requirement for non-linear materials used to absorb currents along the feed line. In turn, this significantly improves performance in the naturally resonating dipole band while only slightly reducing bandwidth as compared to its ideal center-fed counterpart.

1.2 Motivation

The motivation of this research is to provide an antenna design and address some of the issues with respect to radiated currents along the feed line. Several simulation methods are used to validate the design and the solution is segmented into individual components for in-depth analysis and optimal performance. Measurements are performed to confirm the results of the full model simulation.

This research will focus on a resonant choke design for single or stacked dipole antenna configurations. A hybrid numerical model is constructed using Method of Moments and circuit approximation for this quasi-static problem. The numerical model of the choke geometry is given in figure 1.3 and describes both the internal and external networks to be solved for this high power antenna. The geometry is made symmetric as to keep currents symmetric about the center feed.

A study of current technologies including the inductive coil, large impedance step, and absorber materials is also considered. Due to other problems that may exist with some non-linear absorber types [41] or freely radiative coils [15], an enclosed resonant choke solution is pursued.

1.3 Research Objectives

Most texts simply model the half wave finite diameter dipole as a centre fed dual radiator antenna without taking much consideration into the real feed network. A direct procedure is missing to be sure currents are not coupled onto the coaxial feed, which can propagate either into the far field or onto other nearby radiators.

This research develops a fast and accurate numerical model of a dipole antenna with a cylindrical feed support structure entering from either end of the radiator elements in a single or stacked dipole configuration. The model is split into two main sections; namely, the closed model feed network and the radiator elements. A model of the complete lower half of the resonant choke antenna geometry is provided in figure 1.3. The feed and radiator networks are analysed together to determine VSWR and radiation parameters as shown in the block diagram in figure 1.2.

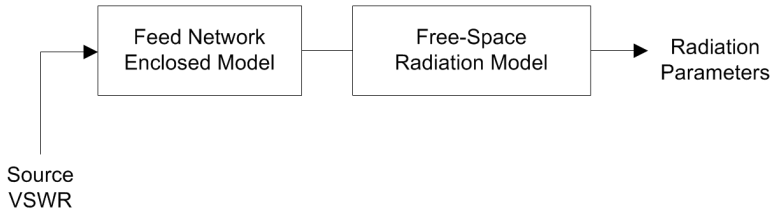

Figure 1.2: Antenna Block Diagram

Both subnetworks have been researched and designed to optimize the performance of the full model while taking into consideration all radiator currents. These two models simplify the design efforts to converge performance to the ideal antenna model.

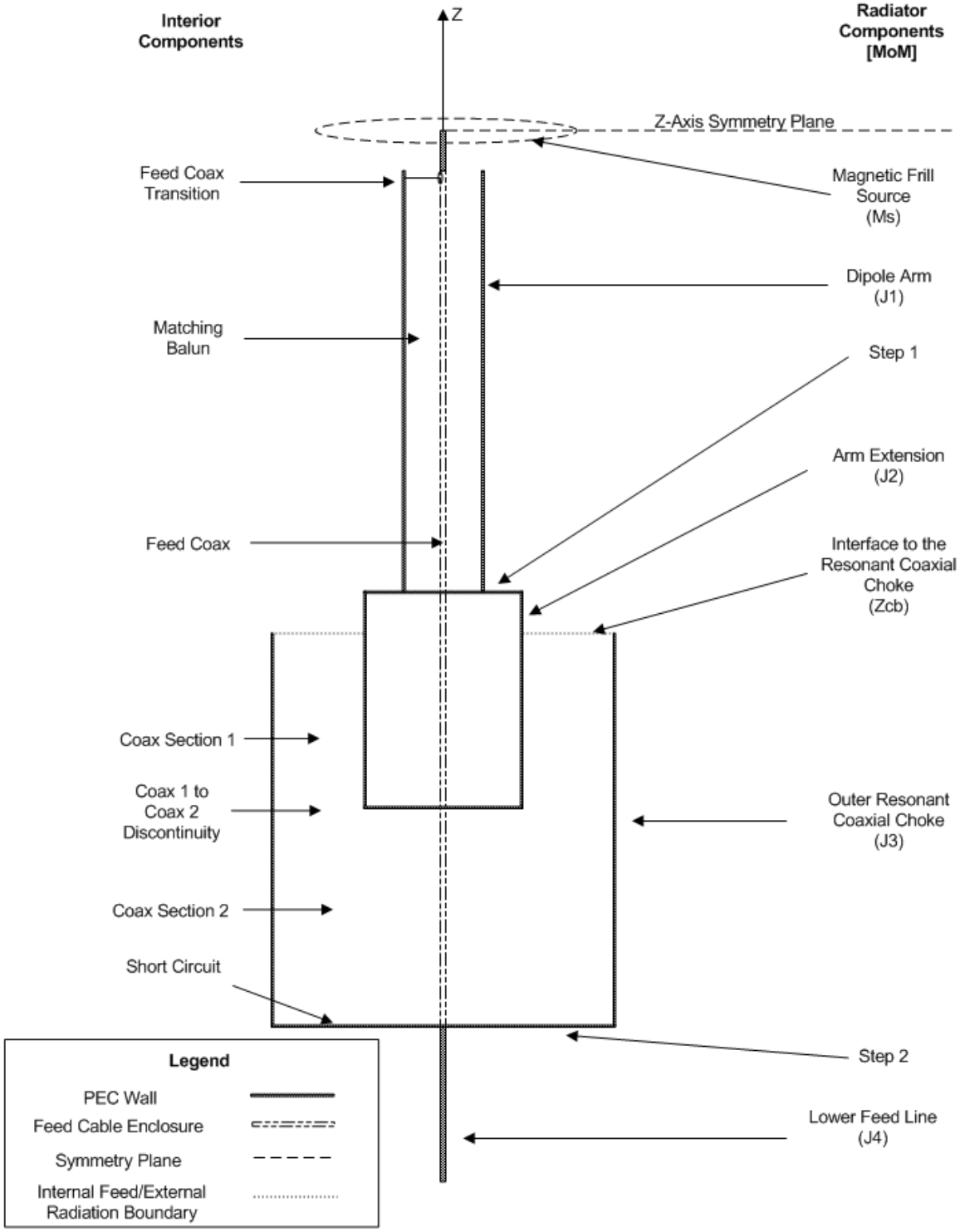

Figure 1.3: Antenna Mechanical Model

1.4 Thesis Organization

The organization of this document is sectioned by chapter. The content of each chapter is specified as follows.

Chapter 1 contains an introduction to the research objectives.

Chapter 2 provides an in-depth literature study. A theoretical analysis of the complete current choking solution is developed leading to a numerical implementation. This is the basis for the numerical methods algorithm used in the discussion of future chapters. A review of numerical errors is also given at the end of this chapter.

Chapter 3 validates the MoM code using simple structures with solutions obtained using analytical formulas and FEM codes. This includes the expected performance of the core antenna elements including the dipole of finite radius and matching balun design. It also covers overall antenna design including the feed line current choke. Validation of the general MoM antenna model using FEM solvers is completed.

Chapter 4 compares the antenna prototype assembly measurement results with numerical solutions. Design for Manufacturing (DFM) procedures are detailed as well.

To conclude this research, chapter 5 covers lessons learned, a research summary, and future research possibilities.

Chapter 2

Theoretical Analysis and Simulation

2.1 Introduction

In order to have an efficiently radiating antenna, both the enclosed feed network and free space radiation elements must be evaluated individually. In this chapter, the dipole radiator elements are analysed, which includes the outer conductor of the coaxial feed line.

Reflection of voltage due to mismatch and unwanted currents coupled onto the feed or other conductive elements can severely degrade performance. Therefore, the matching feed balun, tuning element, and all exterior elements must be taken into consideration in the full antenna design.

The following section reviews published literature on solutions that progress towards a fully integrated resonant choke dipole. Other implementations to minimize feed currents are also studied. This research will allow the designed antenna performance to approach that of its ideal center fed theoretical counterpart.

2.1.1 Current Choking Solution

In a textbook analysis of a cylindrical dipole antenna, the feed network is generally ignored. It is assumed that the source is located at the center of the dipole. Not only does this cause a problem with simulating the actual performance of the antenna, but also causes issues when measuring real performance. This is due to near field radiator currents propagating down the feed line and radiating out into the far field, which is significant for mostly omnidirectional antennas [30].

To isolate the feed network from the radiator, a resonant choking structure is implemented. In general, the current choke must be designed while taking the antenna's near field radiation into consideration. First, the resonant choke structure is studied.

Resonant Choke

The resonant choke is a purely metallic device that prevents leakage currents to travel down the feed line and radiate destructively to degrade antenna far field performance. When not present, reduced performance is expected in the theta cut-plane of the dipole antenna [21]. It has been demonstrated that some current choking structures are highly resonant in nature when placed near the radiating element and are used effectively to isolate other radiators or metallic surfaces. Antenna tunability is mostly dependant on the position and dimension of the resonant choke [38].

To prevent passive intermodulation, the antenna is constructed from entirely metallic surfaces with no dielectrics. If solder joints and welds are done carefully, this allows near-by antennas to radiate at other frequencies without the concern of modulated carrier products to land inside other receive bands [41]. Multiple stacked antennas can also be constructed to radiate multiple bands from the same antenna support structure or with separate feeds [3]. This also allows the antenna to support high power operation [50].

Both the absorber and metallic choke have been verified through measurement and can be visualized in figure 2.1. This figure illustrates the magnetic field distribution of both types of metallic choke and absorber methods using a patch antenna. It is observed that the folded structure of the current choke geometry reduces currents significantly and can have a similar or greater effect than the ferrite absorber method at resonating frequencies. This implementation does not take into consideration the overall antenna radiation characteristics and since it has not be designed to be integrated into the patch radiator, radiation performance can still be significantly reduced in comparison to predicted RF performance.

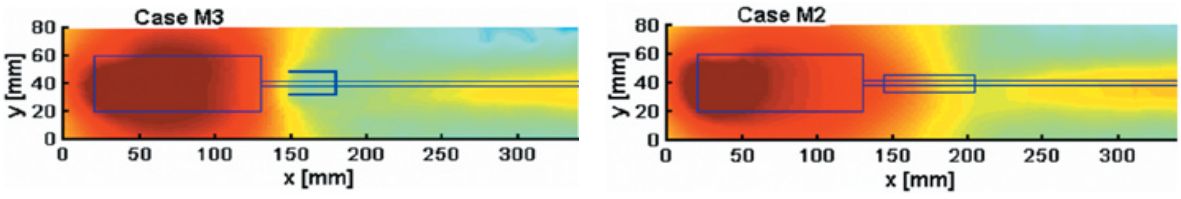

Figure 2.1: Current Choke and Absorber Magnetic Fields for Patch Antenna [21]

A resonant choke structure must be integrated with the radiator. In literature, currents inside the choke are very low with respect to the currents along the main radiators. To enhance the performance of the dipole, the internal choke structure is used to resonate with the antenna. This method creates a large effective inductance at the choke boundary. Since currents resonate within the choke geometry, current located on the outer radiator portion of the choke tend to zero. The full radiative numerical model is shown on the right side in figure 1.3.

In contrast to the resonant choke, other types of chokes can be implemented by simply adding an impedance step or coil inductance between the largest radiator and the feed or other radiators. This helps prevent near fields from coupling onto the line, but requires a very large radiator [50] or large inductive element. Since the choke geometry is smaller in length than the dipole arm length, this is implemented as part of the design between the resonant choke and the feed line/support structure as shown in figure 1.3 as 'step 2', but is not the core method to reduce currents at the edge of the dipole arm.

The resonant choke solution has been implemented to create a band reject filter type structure by using a folded balun inside an enclosed coaxial type device, which supports the feed coaxial line [18]. This, however, does not address currents accumulating on the outer cylindrical conductor and propagating onto other metallic elements, which shifts radiation performance. Other implementations demonstrate a folded choke that extends inside part of the radiator. This works well when the radiator radius is quite large; otherwise, near fields are still trapped on the feed line or support structure [50].

To explore the possibility of using a resonant choke to reflect select frequency bands back onto the radiators, the complete antenna is modelled as a circuit. It is possible to accurately model the dipole pairs as a transmission line [44]. This theory is used to model the entire antenna as a quasi-static KVL circuit. Using the method of moments numerical solution, the coaxial resonant choke can be easily inserted in the dipole antenna model.

Internally, the geometry of the choke structure can be modelled as a stepped coax structure as depicted in figure 2.2. It is numerically modelled using lumped element transmission line theory. This is shown as an enclosed microwave component consisting of two coaxial lines, a coaxial step discontinuity, and a short at one end which makes it act like an enclosed coaxial resonator. Radiative currents are not required to be computed in this structure because it is enclosed. Thus, there is no worry of it radiating into free space. Only the effective input impedance at the interface is required to add to the MoM model to compute currents along the exterior radiator, which is amplified by the resonant nature of this type of choke.

The inner choke radius is designed to be larger than the dipole arms to add to the

overall boundary inductance. This has an implementation limit since the outer conductor of the choke cannot be too large. The characteristic impedance is reasonably designed to match the radiator. The step discontinuity at the midpoint of the choke acts as a large capacitance or a large inductance at the Zcb boundary, which pushes the support radius to be small. Resonant effects of this choke also are observed to add additional inductance at the boundary interface due to the structures' approximate quarter wave reflection characteristics.

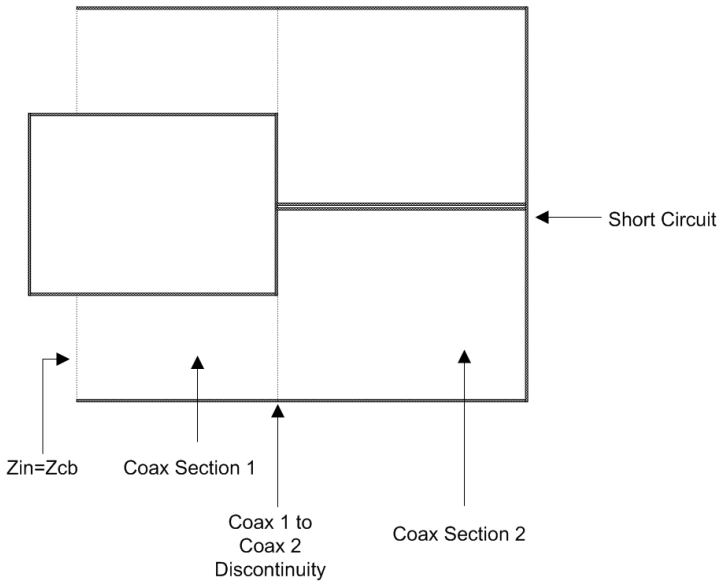

Figure 2.2: Choke Geometry Diagram

Although they are not as effective, inductive steps, coils, and absorber solutions can also assist with choking currents along the feed line. Their advantages and disadvantages as compared to the resonant choke structure is studied.

Absorber Solution

The ferrite absorber can act relatively efficiently as a current absorber. While there can be improvements to ferrite absorbers by different manufacturing techniques, this type of solution is used as a comparison to the metallic resonant choke solution.

There are many advantages to using an absorber to reduce the magnetic field strength on the feed line. Due to their wideband absorbing characteristics in VHF band, dipole

antennas can be tuned without too much effort. These absorbers may offer a compact and somewhat lightweight option.

However, ferrite absorbers are non-linear in nature. Due to the fact that most antenna installations have a passive intermodulation requirement coupled with the probability of many microwave sources in relative proximity to the installation site, a purely metallic solution is preferred to allow better control of this phenomenon.

An absorber could be installed as in figure 2.3 to prevent currents from continuing onto the feed. This has proven to be very effective to allow correction to radiation characteristics and VSWR [43, 23].

Figure 2.3: Current Absorber at Dipole Ends

Although the current absorption is highly dependant on the material properties, an attempt is made to simulate these materials on the dipole structure in a typical case. The results of the simulation study are presented in chapter 3 for the purposes of a comparitive study. In addition to the resonant choke and ferrite absorbers, impedance step and inductive coil solutions also have been considered.

Impedance Step and Inductive Coil Solution

Large impedance steps and inductive coils are frequently used to isolate the feed network from the radiating element or stacked dipole antennas. Due to the quasi-static nature of VHF/UHF dipole antennas, impedance steps or inductive coils can be used as a simple non-resonating current choke to try and isolate currents from the radiator elements. This typically works best when frequency bands are close. Inductive coils have a significant effect on the wideband match of the overall antenna; however, current distributions are seen to significantly shift antenna directivity due to the accumulation of currents on other areas of the radiator [15].

Essentially, the additional current density on other elements are the root cause of the shifted far field radiation problem. This can be seen by the current distribution plot of a resonating frequency for one resonating element. The current distributions in figure 2.4 shows the radiating dipole along with strong leakage currents forming on the other radiator elements. Ultimately, the leakage currents on other resonant elements could be formed on the feedline.

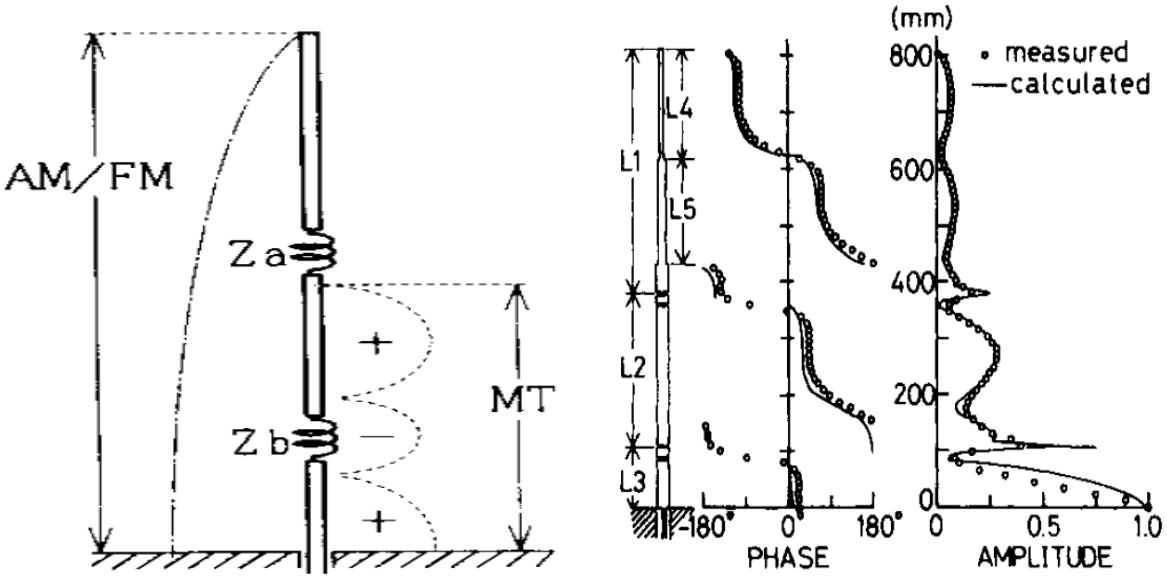

Figure 2.4: Current Distribution of a Coil Loaded Dipole Array (left: Antenna Geometry right: Current Distribution) [16]

It is clearly visible from figure 2.5 that leakage currents onto other radiator resonating elements affect the far field radiation patterns [16]. In terms of antenna radiation performance, these leakage currents can cause a significantly shifted and reduced performance in comparison to the antenna's ideal model.

In comparison to the resonant choke solution, the resonant choke dipole antenna will lose bandwidth due to the resonant effect of the entire structure (ie: the antenna's Q-factor will increase). It has been found that inductive coils can increase bandwidth if the coils are moved to the dipole radiator ends due to the additional current charge density there. When unshielded, this has a significant effect on radiation characteristics. However in the resonant choke model, the coaxial diameter increases to add to the charge accumulation effect and increase inductance. This does not disturb the antenna radiation characteristics

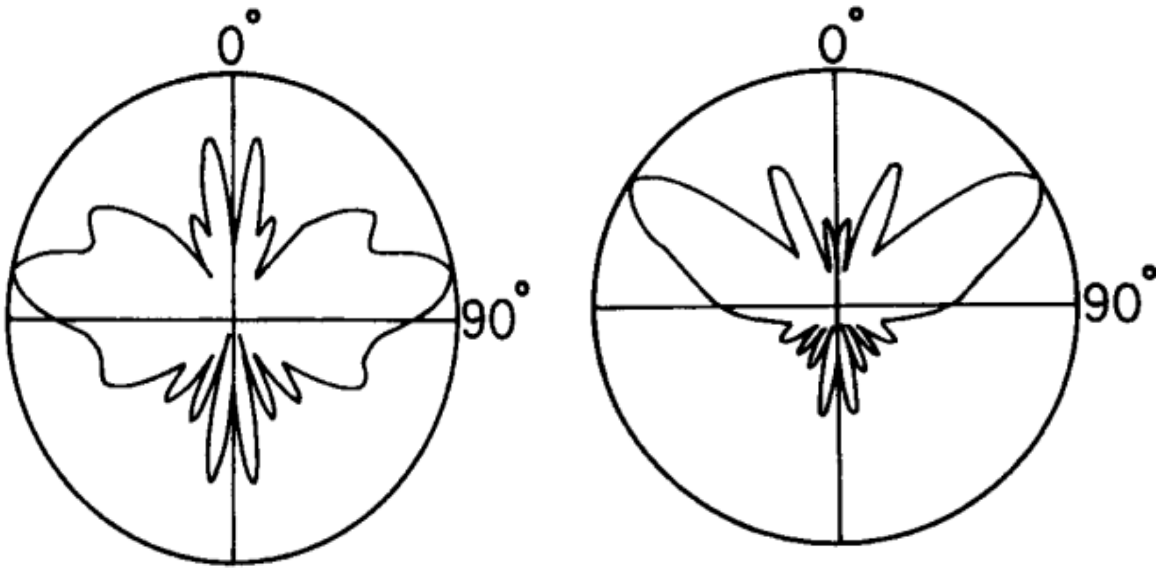

Figure 2.5: Shifted Radiation Patterns Due to Leakage Currents [16]

since the additional currents are enclosed by the resonant coaxial structure structure as shown in figure 2.2 above.

2.1.2 Simulation Tools using Numerical Analysis

As in other typical antenna problems, several simulation tools may be used to simplify or solve an antenna problem more efficiently. Greater depth to understanding sources of error or fundamental knowledge of the problem by splitting the problem into parts allows for design innovation. In this research, the final numerical model is assembled systematically by combining the radiation model with the feed scattering parameter matrices produce the antenna's overall characteristics, as illustrated in figure 2.6.

Each section of the antenna problem may be solved using several simulation tools. In theory, FEM may be used to solve the complete problem. This, however, can be quite demanding in terms of computational resources. To analyse and optimize the overall antenna problem, each section is solved using its best-known numerical technique. This allows for a quick design of independent problems and assemble the complete problem with little final optimization.

Due to the nature of the problems given by the code developed and results produced by commercial electromagnetic (EM) solvers, Matlab is frequently used to easily and efficiently manipulate numerical matrices to solve radiation problems and combine overall scattering parameters [46]. Numerical electromagnetic simulators used to compute the theoretical antenna performance in a vacuum space have their own advantages and disadvantages. These will now be discussed.

2.2 Radiator Numerical Solvers

Both Method of Moments (MoM) and Finite Element Method (FEM) solvers are used to solve and optimize the antenna solution. Both numerical solvers offer advantages and disadvantages in terms of speed versus accuracy [24]. In this research, the most efficient way to solve radiation problems, while taking the near field into account, is by using symmetry. In this case, the Method of Moments offers many advantages to quickly and efficiently solve the free space antenna problem. This inspired a custom MoM code to be written in Matlab to research the effect of different configurations. Other efficient codes using axial symmetry about the center axis parallel to the radiator include commercially available FEM codes such as Comsol Multiphysics [14], but still use larger matrices to solve the same problem.

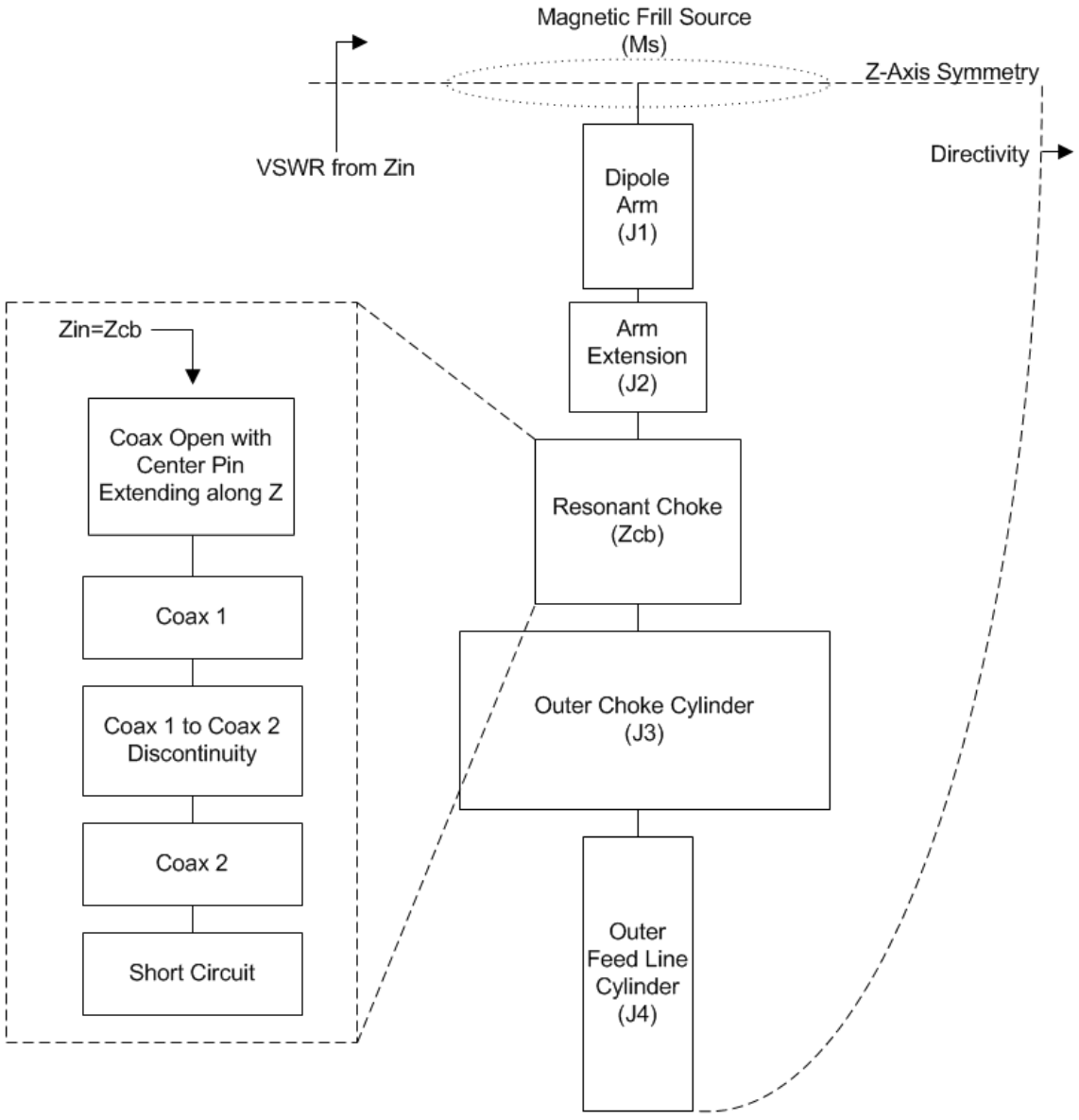

Figure 2.6: Antenna Solution Block Diagram

2.2.1 Method of Moments Mathematical Model

We start the Method of Moments analysis by segmenting the radiator into its most simple form. That is, a cylindrical scatterer with sections of changing radii [20]. Each of the antenna sections are labeled as J_n, as depicted in figure 2.7.

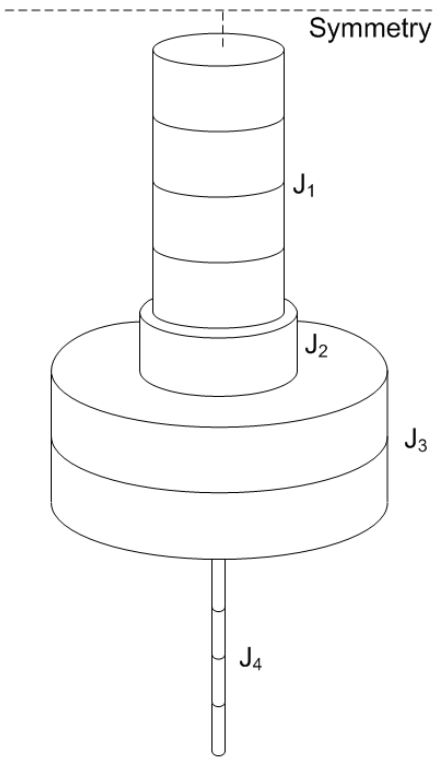

Figure 2.7: Segmented Dipole Antenna Model

The cylindrical radiating surface is assumed to be PEC so that [7]

$$\vec{E}^t = \vec{E}^i + \vec{E}^s = 0 \tag{2.1}$$

where $\vec{E}^i$ and $\vec{E}^s$ are the incident and scattering electric field vectors respectively. The scattering electric field is used to compute impedance along the cylindrical scatterer. It can be derived from the vector potential $\vec{A}$ for which

$$\vec{A}^2 + k^2\vec{A} = -\mu\vec{J} \tag{2.2}$$

using the standard Lorentz condition on Maxwell's equations. The above equation can be solved for $\vec{A}$ to obtain the relation

$$\vec{A} = \frac{\mu}{4\pi}\iiint_V \vec{J}\frac{e^{-jkR}}{R}dV'. \tag{2.3}$$

where $G(z,z') = \frac{e^{-jkR}}{R}$ is known as the free space Green's function [20]. Using the scaler and vector potentials, Maxwell's equation for $\nabla \times \vec{E}$ can be reduced to its differential form

$$\vec{E}^s = -j\omega(\vec{A} + \frac{1}{k^2}\nabla(\nabla \cdot \vec{A}). \tag{2.4}$$

While neglecting edge effects and only considering the radiating surface, the above equation can be reduced to it's scalar form

$$E_z^s = -j\frac{1}{\omega\mu\epsilon}(k^2A_z + \frac{\partial A_z}{\partial z}) \tag{2.5}$$

with A_z computed as

$$A_z = \frac{\mu}{4\pi}\iint_S J_z\frac{e^{-jkR}}{R}dS' \tag{2.6}$$

where $R = (\rho^2 + a^2 - 2\rho a\cos(\phi - \phi') + (z - z')^2)^{1/2}$ and $\phi = 0$ for this axisymmetrical problem. Also note that primed and non-primed values indicate source and field points respectively. It is now possible to combine equations 2.5 and 2.6 to produce the scattering field integral equation

$$E_z^s = -j\frac{1}{\omega\mu\epsilon}(k^2\frac{\mu}{4\pi}\iint_S J_z\frac{e^{-jkR}}{R}dS' + \frac{\partial}{\partial z}\frac{\mu}{4\pi}\iint_S J_z\frac{e^{-jkR}}{R}dS'). \tag{2.7}$$

The free space magnetic field can be computed from Maxwell's equations [24]

$$\vec{H} = -\frac{1}{j\omega\mu}\nabla \times \vec{E} \tag{2.8}$$

and the line current down the PEC radiator can be computed from the following vector equation

$$\vec{J_s} = \hat{n} \times \vec{H}, \tag{2.9}$$

or in the scalar form

$$|J_z| = |(\hat{n} \times \vec{H}) \cdot \hat{z}| = |(\hat{x} \times \vec{H}) \cdot \hat{z}|. \tag{2.10}$$

In the second term of equation 2.7, the partial derivative and the integral can be interchanged to combine both integrals. Also, if a is kept small enough, the assumption that $\rho = a$ can be applied. It is a rule of thumb that $a << \lambda$ [7]. This will be a source of error in the Method of Moments code, which is discussed later in the chapter. E_z^s then becomes

$$E_z^s = -j\frac{1}{\omega\mu\epsilon}\int J_z \frac{e^{-jkR}}{4\pi R^5}[(1+jkR)(2R^2-3a^2)+(kaR)^2]\,\mathrm{d}z'. \tag{2.11}$$

It can be noted here that the above equation will need to be solved by segmentation due to the J_z term. This allows for the J_z term to be extracted from the integral as a constant term for each segment of the antenna. The antenna radiator segmentation is shown in figure 2.7 above. It is also noted that surface current term can be substituted with the location of the impedance term at the center of the radiator by reciprocity. This allows for the ρ in the equation for R to be zero, which leaves $R = (a^2 + (z-z')^2)^{1/2}$.

Solving equation 2.1 for $\vec{E}^i$, equation 2.11 can be solved for the incident field that is now located at $\rho = a$

$$I_n(z_n')\int_{\delta_n} \frac{e^{-jkR}}{4\pi R^5}[(1+jkR)(2R^2-3a^2)+(kaR)^2]\,\mathrm{d}z' = -j\omega\epsilon E_z^i(\rho=a). \tag{2.12}$$

where n is the segment number along the radiator. The above equation is a convenient form to compute filament line currents along the radiator [7].

A virtual coaxial source is used as a field potential E_z^i with $\rho = a$ as the center conductor radius and the outer conductor defined by the impedance required at the source. This virtual source is depicted in figure 2.8. The gap given by [51]

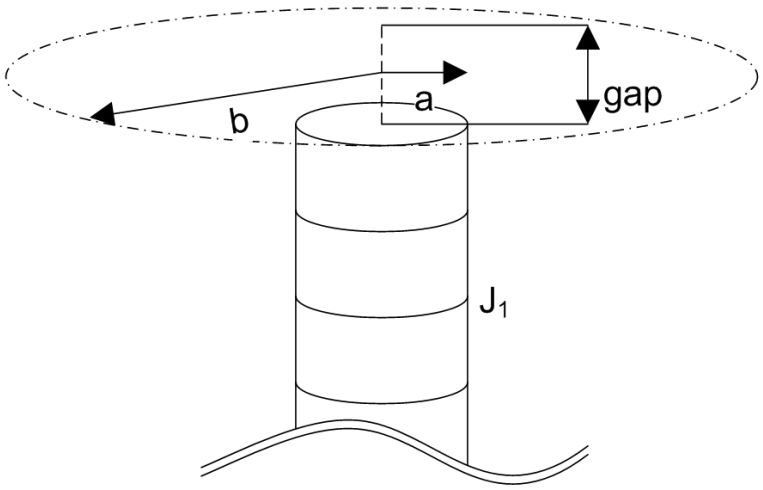

Figure 2.8: Source Definition

$$E^i \simeq -V_s(\frac{k(b^2-a^2)e^{-jkR}}{8log_e(\frac{b}{a})R^2}(2(\frac{1}{kR}+j(1-\frac{b^2-a^2}{2R^2})) \\ +\frac{a^2}{R}((\frac{1}{kR}+j(1-\frac{b^2+a^2}{2R^2}))(-jk-\frac{2}{R})+\frac{-1}{kR^2}+j\frac{b^2+a^2}{R^3}))) \tag{2.13}$$

The above equation can be simplified for electrically small radii, which removes the ρ dependence. Therefore, the new applied electric field is given as [51]

$$E^i = \frac{-Vs}{2\log(\frac{b}{a})}(\frac{e^{-jr_1}}{r_1}-\frac{e^{-jr_2}}{r_2}) \tag{2.14}$$

where $r_1 = (z^2+a^2)^{(1/2)}$ and $r_2 = (z^2+b^2)^{(1/2)}$. The applied electric field E^i or more simply, the segment source voltage $[V_m]$, is defined as a field applied along the length of

the radiator. The source input is defined as magnetic frill located at the centre of the dipole. It can be defined either with or without ρ dependence given the symmetry of the problem [51]. Should the geometry be more complex, higher order modes above TEM may be added to reduce the error of the applied electric field [20, 11].

The equation 2.12 can be reduced to the form

$$\sum_{n=1}^{N} I_n(z'_n) Z_n = -E^i, \tag{2.15}$$

where N is the total number of segments along the radiator, I is the segment current, Z_n is the segment impedance, and E^i is the source.

In this case, a KVL method is most conveniently used by computing impedances along the radiator surface [44]. This allows for internal structures to be added to the radiator impedances. The equation 2.15 as shown in figure 1.3 can then be implemented in matrix form as

$$[I_n][Z_{mn}] = [V_m], \tag{2.16}$$

where $[V_m]$ is defined as the applied electric field along each segment of the radiator, $[Z_{mn}]$ is the impedance, and $[I_n]$ is the unknown current distribution. In this form, internal coaxial choke Z_{in} impedance can be inserted into its respective $Z_{m,n}$'th element. Solving the above equation, the final solution is quite simply

$$[I_n] = [Z_{mn}]^{-1}[V_m], \tag{2.17}$$

and $[Z_{mn}]$ can be expanded as a 2D matrix from a 1D segmentation $[Z_k]$ along the radiator as follows

$$Z_{m,n} = \begin{pmatrix} Z_1 & Z_2 & \cdots & Z_k \\ Z_2 & Z_1 & \cdots & Z_{k-1} \\ \vdots & \vdots & \ddots & \vdots \\ Z_k & Z_{k-1} & \cdots & Z_1 \end{pmatrix} \tag{2.18}$$

for Z_1 starting at $-l/2$ and Z_n ending at $l/2$ and $[Z_k]$ defined as

$$[Z_k] = \int_{\delta_n} \frac{e^{-jkR}}{4\pi R^5}[(1+jkR)(2R^2-3a^2)+(kaR)^2]\,\mathrm{d}z'. \tag{2.19}$$

2.2.2 Matlab Implementation

The current can be numerically computed at each segment of the radiator using 2.17. Matlab is used to implement matrix equations 2.17, 2.18, and 2.19 with the source defined in equation 2.14. The commented source code is given in appendix I. Some useful open-source tools for electromagnetics were found on the matlab webpage [34] and also in other open-source packages [39].

Packages used to convert [ABCD], impedance, and scattering parameter matrices allowed quick system design for the overall antenna. See Appendix I for additional details concerning antenna system computation.

Coaxial Line

Typically, the dipole antenna is connected to the transceiver with a coaxial cable. From chapter 2, the ABCD parameters of a lossy coaxial can be easily computed numerically and inserted into the overall antenna system. These computed scattering parameters are combined directly with the antenna Balun.

Additionally, the coaxial cable not only acts as the feed line that carries energy to the radiator, but its outer conductor also re-radiates RF energy from currents coupled by the antenna's near field. As a design goal, a cylindrical support structure is designed to enclose the feed cable inside. The support pipe isolates the feed coaxial cables from coupled current. This also provide a rigid structure to attach the dipole to the support structure as shown in figure 1.3.

For the straight coaxial sections, the ABCD parameters can be computed using the dimensions of the waveguide. The ABCD parameters are given by [42]

$$[ABCD] = \begin{pmatrix} \cos\beta l & jZ_0\sin\beta l \\ j\frac{1}{Z_0}\sin\beta l & \cos\beta l \end{pmatrix} \tag{2.20}$$

with β and Z_0 defined as the the waveguide propagation constant and the waveguide impedance respectively. β and Z_0 can be computed from the transmission line characteristics of a coaxial line. This is given by [42]

$$Z_0 = \sqrt{(}\frac{R + j\omega L}{G + j\omega C}) \tag{2.21}$$

$$\beta = \sqrt{((R + j\omega L)(G + j\omega C))} \tag{2.22}$$

where for a coaxial waveguide

$$L = \frac{\mu}{\pi} \log_e(\frac{b}{a}), \tag{2.23}$$

$$C = 2\pi \frac{\epsilon'}{\log_e(b/a)}, \tag{2.24}$$

$$R = \frac{1}{2\pi\sigma \tan\delta}(\frac{1}{a} + \frac{1}{b}), \tag{2.25}$$

$$G = 2\pi^2 f \epsilon'' \log_e(\frac{b}{a}). \tag{2.26}$$

Resonant Choke Circuit Model

To insert the choke model into the MoM code, a circuit model is used. The coaxial choke structure is analyzed by combining the scattering and impedance parameters of each of the individual components [46]. A general circuit model of this device is shown in figure 2.10. Since the waveguide between discontinuities is somewhat electrically large, a simple circuit approximation of the coaxial step discontinuity is used [47]. More accurate models can be modelled by the Mode Matching method should the geometry extend out of the usable range of the circuit approximation [40]. The capacitance of the coaxial circuit model discontinuity is given by

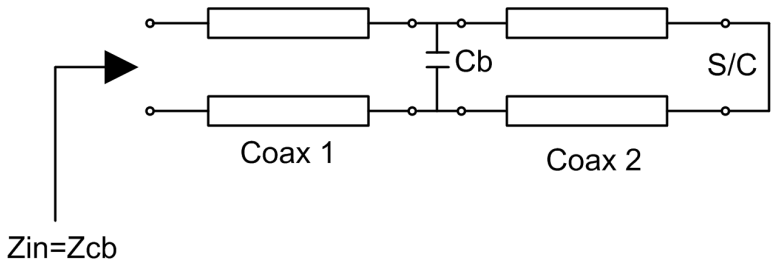

Figure 2.9: Choke Circuit Diagram

$$C_b = \frac{\epsilon}{\pi}[\frac{\alpha^2+1}{\alpha} log_e \frac{1+\alpha}{1-\alpha} - 2log_e \frac{4\alpha}{1-\alpha^2}]. \tag{2.27}$$

The resonant characteristics of this shorted structure of the coax 2 section adds significantly to the effective inductance at the interface boundary. The resonant section is inserted using a parallel resonator configuration as shown in figure 2.10 where Z_{res} is given by

$$Z_{res} = (\frac{1}{j\omega L_r} + j\omega C_r)^{-1}. \tag{2.28}$$

Finally, the addition of all impedances and transmission lines are used to compute the Zin of the resonant choke model. This frequency dependant value is inserted into the choke resonator discontinuity point of the MoM numerical code.

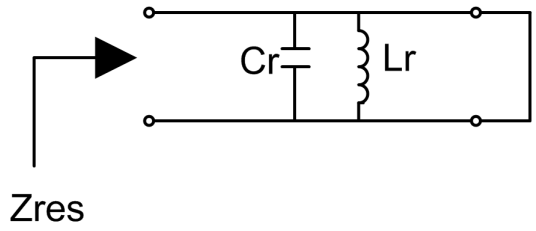

Figure 2.10: Resonant Circuit Model

As an additional note, the interface to the choke component can be thought of as an infinitely long centre conductor protruding out of the coaxial line. Higher order fringing fields at the interface of this model can be expected, but are assumed small in this model [8]. This could be another source of error.

2.3 Feed Network Analysis

In this section, the antenna feed network is analysed as individual components leading to the radiator. The feed model will be composed of a coaxial line, a matching transformer, and finally the antenna matching balun as shown in figure 2.11. These items will be discussed in the following sections.

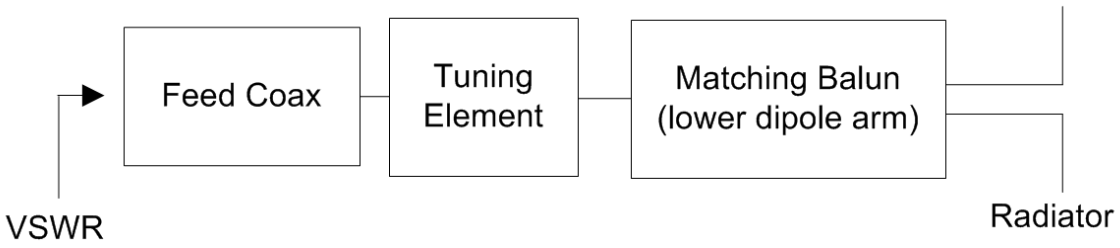

Figure 2.11: Dipole Antenna Block Diagram

2.3.1 Antenna Balun

Every dipole antenna has a balun to rebalance the TEM coaxial fields before dipole radiation. In this case, a quarter-wave section of coaxial waveguide is used to balance the naturally unbalanced TEM guided center conductor and outer conductor. The cable isolator acting as the feed conductive shell is used as part of the antenna balun similar to that of a type II sleeve balun design and shown in figure 2.12[37]. The feed cylindrical enclosure is best fit as a center feed due to its symmetry about the antenna's center axis. This will result in symmetrical antenna directivity about ϕ.

The interface to match the antenna to the network analyzer is a 50Ω coax cable. Ideally, since the antenna input impedance is near 73Ω, an impedance matching section will be required to provide the transition to the coax cable. A 75Ω coaxial cable is used to simplify the design. This impedance step will be integrated into the balun transition. The return

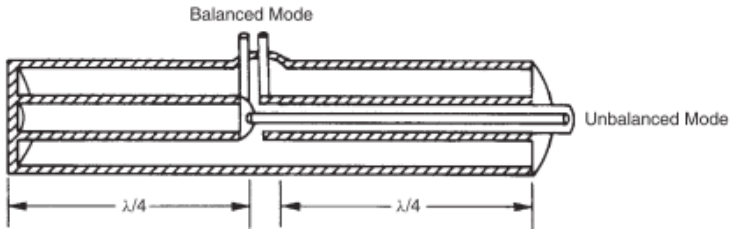

Figure 2.12: Design Based on Type II Sleeve Balun [37]

loss goal of the this section is also made low enough to be sure the performance of the balun does not affect the overall antenna performance.

To step from the coax feed cable to the outside radiators, an internal coax structure was designed as shown in figure 3.20. The design was kept simple as an air filled coax that needed to be near the ideal impedance of a dipole. The results are presented in Chapter 3.

2.3.2 Tuning Element

A tuning element can be used to match the radiator input impedance over a wider frequency range. In this case, a simple stub tuner is designed and inserted just before the balun [42]. The advantage to using a stub tuner is its compact shape. It is implemented by soldering a shorted coaxial cable to the main coaxial feed line at a distance from the source point.

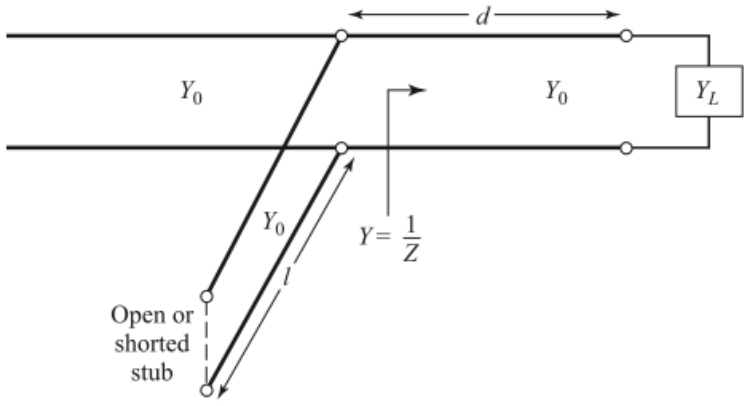

Figure 2.13: Tuning Circuit [42]

Once the initial measurements of radiator and balun are complete, the s1p file generated is used with the coaxial cable characteristics in a circuit simulator to match the antenna over a wider frequency band.

2.4 Sources of Error

Several different solvers are used to examine the dipole choke problem and validate the method of moments code. Each numerical implementation has its own advantages and disadvantages with respect to computational efficiency. Since it is never possible to have limitless hardware resources, a discussion of the significant sources of error allows better understanding of the design direction.

Validation of the different simulation methods is required to be certain that measured results will be close to those simulated. Due to the nature of this problem, it is difficult to remove all sources of error in simulation and measurement. The latter is discussed in Chapter 4.

2.4.1 Sources of Error in MoM Codes

As discussed above, it is possible to encounter numerical error with simplified MoM codes. A significant source of error is generated at the radii step discontinuity and resonator L/C values. While developing a robust MoM code that solves the dipole model including the choke, the enclosed coaxial-type structure will have higher order modes generated at the interface. This causes fringing fields in this area that will have a global effect on the antenna problem.

Other sources of error include those found by simplifying the source to be electrically small. This can add significant error to radiators with large radii. In this case, the outer choke surface could contain some sources of error; however, this area is less significant since it is located electrically far from the source and has a low current distribution due to the effect of Z_{cb}.

2.4.2 Sources of Error in FEM Codes

Numerical computational error can be significant for FEM if there is insufficient mesh in the problem. In FEM codes, adaptive meshing allows s-parameters to converge where

fields are changing radically. In particular, HFSS requires manual seeding of radiation boundaries to achieve acceptable results with respect to directivity and gain plots since they are not required for convergence using the default solver values.

In order to guarantee that radiation parameters are converging and computational error is reduced, computation volumes around the antenna should be grown to verify convergence. It is found through numerical experimentation that the radiation boundary should be located approximately $\lambda/2$ away from the largest radiator in the direction of the main lobe for reasonable results.

2.4.3 Sources of Error in Lumped Element Codes

Lumped element codes generally function over a very limited range of geometry. Extending past the recommended working range results in larger error. S-parameters obtained from these codes can be verified using Mode Matching techniques; however, they require significant efforts to implement numerically. Commercial software such as Microwave Wizard or Fest3D may be used in lieu of Lumped Element to add flexibility to the numerical code without sacrificing accuracy or computational speed over FEM codes. These codes could also model the resonator section quite accurately, which improves the overall antenna simulation model.

Chapter 3

Radiator and Feed Network Simulation

The method of moments algorithm is known in the antenna design community as being one of the most efficient methods to solve free-space radiation problems. As shown in the previous chapter, the method can also be used to include internal structure impedances while taking outer geometry radiation characteristics into consideration. This allows the resonant choke internal geometry to be modelled and inserted into the MoM code.

The radiator and feed network simulation models can be implemented using the theoretical analysis defined in the previous chapter. The MoM model is first validated by comparing to a similar FEM model using Ansys' HFSS [5].

3.1 Method of Moments Simulation Model

In both the MoM and FEM center-fed dipole models, the feed network is neglected, which allows some validation before constructing the full antenna simulation model.

3.1.1 VSWR and Directivity of a Finite Radius Dipole Antenna

To validate the MoM code written in Matlab [34], an ideal dipole is computed using the numerical integral equation for a finite diameter cylinder as described in chapter 2. From equation 2.17, the input impedance can be computed by

$$Z_{in} = V_{in}/I_{mid}, \tag{3.1}$$

for which I_{mid} is defined as the segment current computed at the center or midpoint of the radiator.

Once Z_{in} is computed, the input impedance is converted to a reflection coefficient, Γ, and finally to VSWR. Note that VSWR reference impedance is 75Ω in all validation plots, however, a balun is designed for a 50Ω coaxial impedance for the choke dipole antenna. Finally, the ideal current distribution along the radiator is computed for several different lengths. The directivity is then computed and compared to the HFSS model.

3.1.2 Radiator Effective Electrical Length

It is expected that the added radiator geometry to prevent currents onto the feed line will have a significant effect on the electrical length of the dipole arms. An overall smaller bandwidth for dipole arms of similar length compared to its ideal counterpart is expected. To illustrate this effect, the magnitude of the current distribution along the antenna must be visualized. All finite radius dipole lengths are shown in terms of λ where the a center frequency of 125MHz is found for R = 0.9375in, λ = 42in, and Gap = 1in.

Ideally, $|\vec{J_z}|$ tends to zero along the top and bottom of the dipole. This is confirmed in figure 3.1 and 3.3 as the current clearly tends to zero at the ends of the dipole arms for $\lambda/4, \lambda/2$, and λ lengths. This will be the design goal to satisfy the research objectives.

The directivity at center frequency is also compared. It is observed that the error between the plots increases as the arm length increases. This appears to be due to the increased number of tetrahedra in the finite element model with respect to the increase in computational air volume. It has been observed that directivity plots can decrease in accuracy unless a very large air volume is used. This is another advantage to use method of moments since the directivity is derived from the line currents along the radiator while computationally, the surrounding volume is assumed free space.

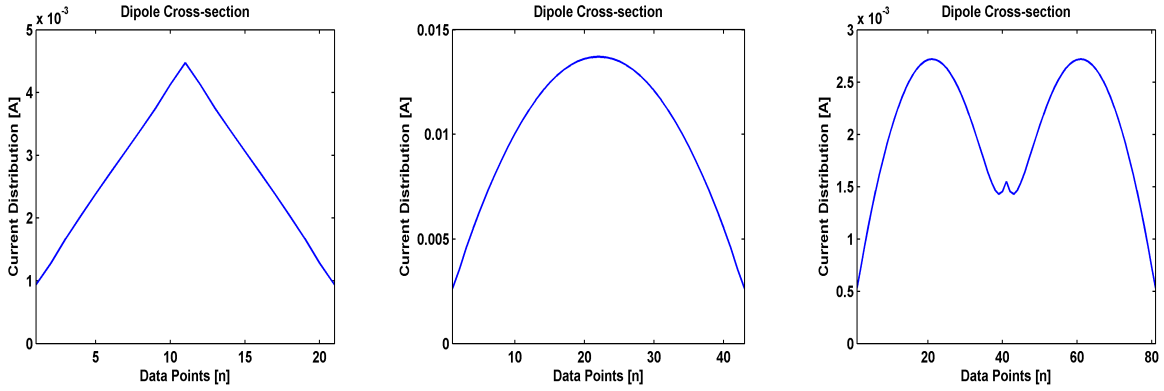

Figure 3.1: MoM Ideal Dipole Current Distribution (left: $\lambda/4$ center: $\lambda/2$ right: λ)

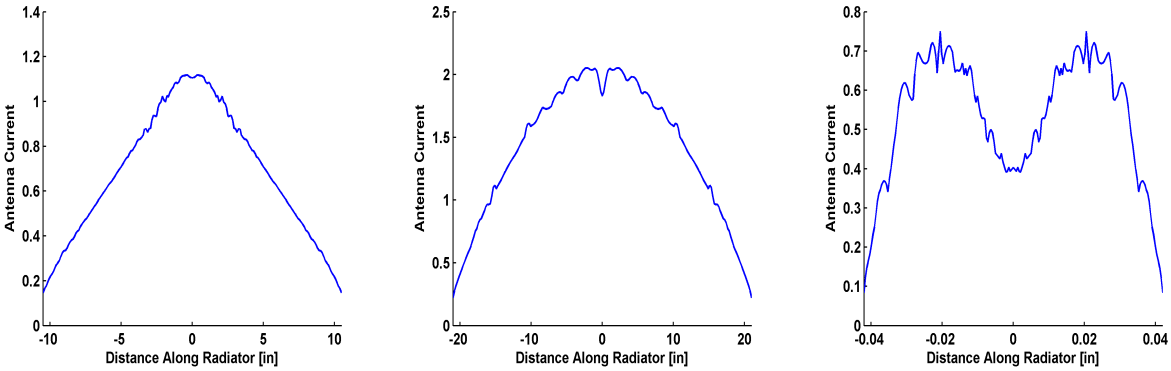

Figure 3.2: HFSS Ideal Dipole Current Distribution (left: $\lambda/4$ center: $\lambda/2$ right: λ)

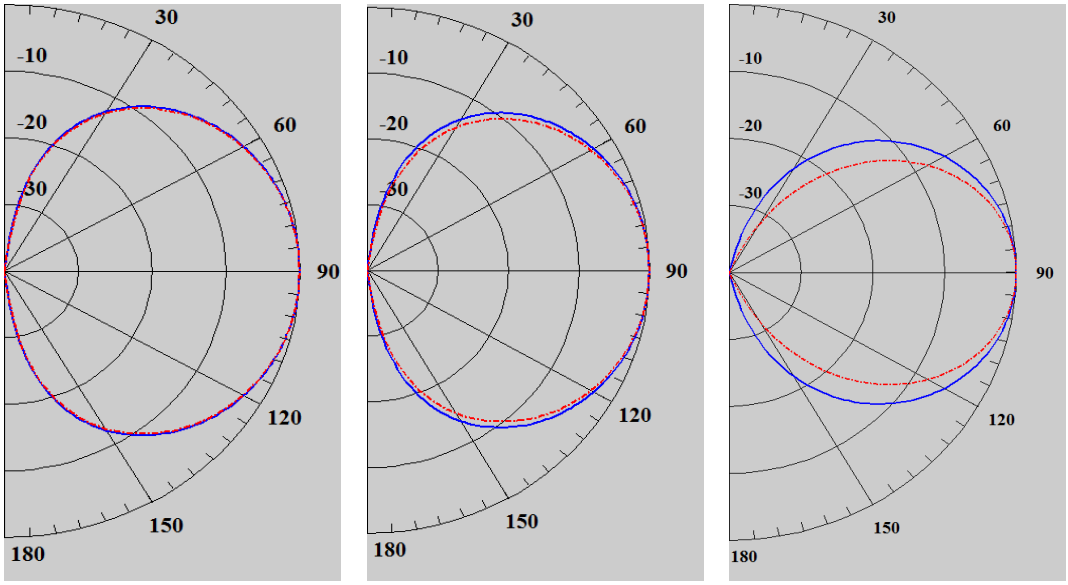

Figure 3.3: MoM vs HFSS Ideal Center-fed Dipole Directivity (left: $\lambda/4$ center: $\lambda/2$ right: λ)

3.1.3 Radius of the Radiator Arms

In theory, the dipole is analyzed for a zero radiator radius, which allows the computation of the exact field equations generated by the antenna [7]. In practice, the radius of the radiator arms is non-zero and must be optimized for a frequency band. The code in Appendix A can be used to compute the antenna parameters of a simple dipole for several different radii. Both VSWR and directivity vs frequency is computed for several radii as shown in figure 3.4. An optimal design is found to be around 1”

3.1.4 Gap Spacing Between Radiators

The gap spacing is also analysed as a design parameter. The resonant frequency can be significantly shifted by manipulating the gap space between the dipole arms. It’s visible from the plots in figure 3.5 that by increasing or decreasing this parameter, the resonance shifts higher or lower in frequency respectively. This can naturally degrade VSWR for gap sizes that are too large.

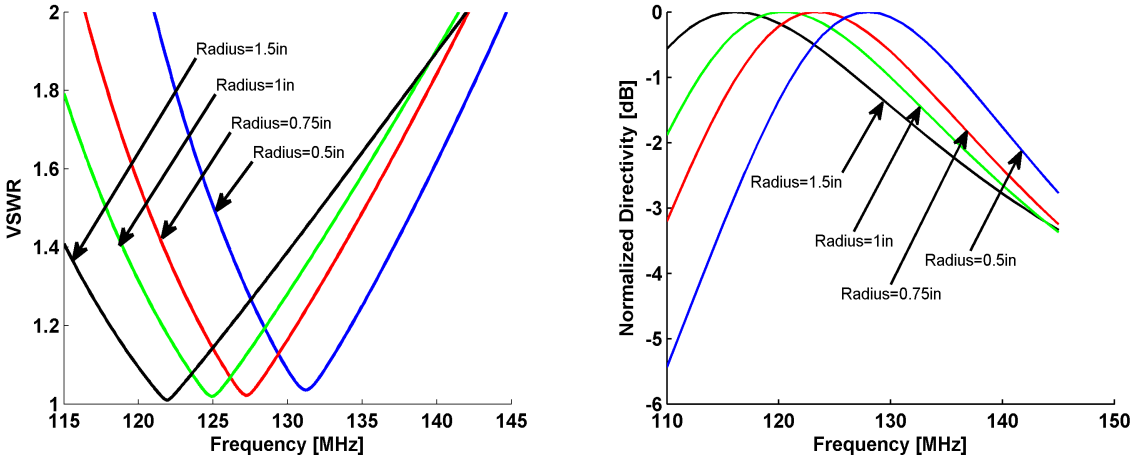

Figure 3.4: VSWR and Normalized Directivity for Several Radiator Radii

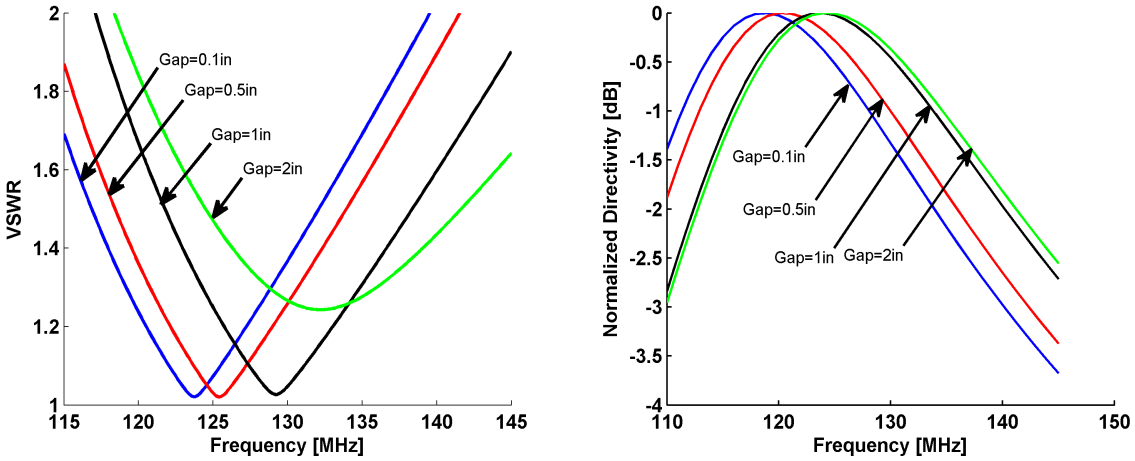

Figure 3.5: VSWR and Normalized Directivity for Several Radiator Gaps

3.1.5 Dipole Comparison Results

The results above show that the radiator arm radius and source gap spacing are both very sensitive parameters. Small perturbations in source modelling by either numerical model results in significant shifts in resonance. This can be seen by setting both the MoM and FEM models with the same geometry and visualizing the antenna performance in figure 3.6.

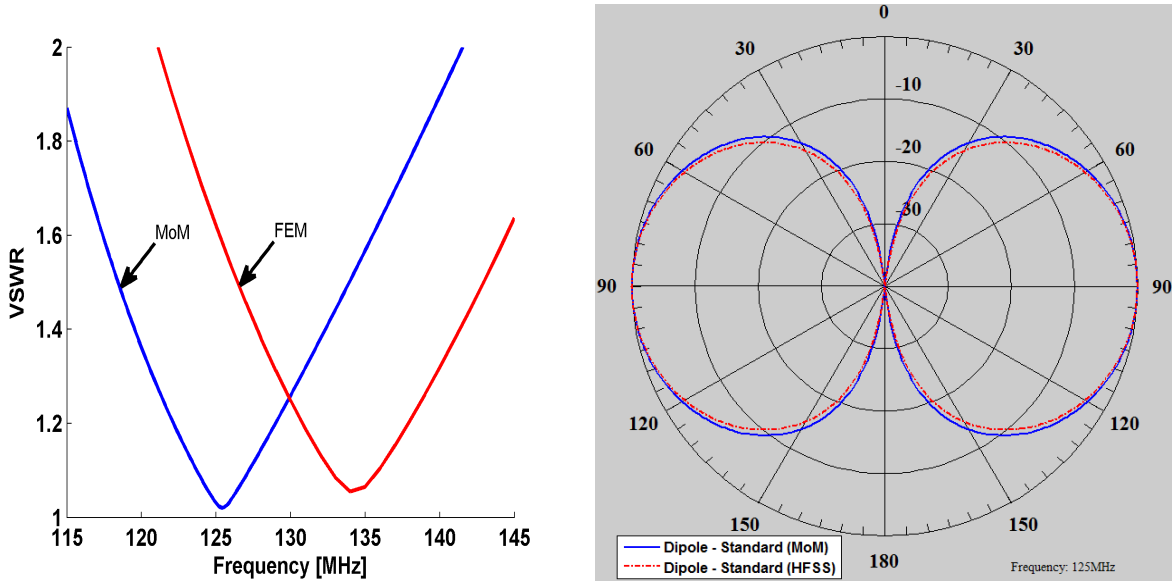

Figure 3.6: VSWR (left) and Directivity (right) of MoM and FEM $\lambda/2$ Dipole Models

Both models use a source impedance of 75Ω, however, we can see that the resonance shift is due to a combination of MoM and FEM computational modelling errors.

3.1.6 Source and Boundary Modelling

To be sure that the simulation is accurate, both the source and all boundary conditions should represent the actual antenna conditions as closely as possible. To keep the radiation model simple, the above simulations are performed using a 75Ω real interface impedance. This is assumed on both the FEM and MoM models. Additionally, an ideal PEC surface boundary conditions are assumed for all metallic surfaces.

Specifically for the FEM model, radiation boundary conditions are given to the limits of the bounding air cylinder containing the antenna geometry. Additional minimum refinement is specified on the radiation boundary to improve accuracy. Although this improves the model, a degradation in directivity performance is shown for this electrically large problem.

3.2 Feed Line Effects

The main purpose of this research is to analyse and prevent the accumulation of feed line surface currents. These surface currents are generated once a metallic line passes near/through either end of any dipole antenna. This is illustrated in figures 3.7 and 3.8 by noting the red color, which indicates large surface currents.

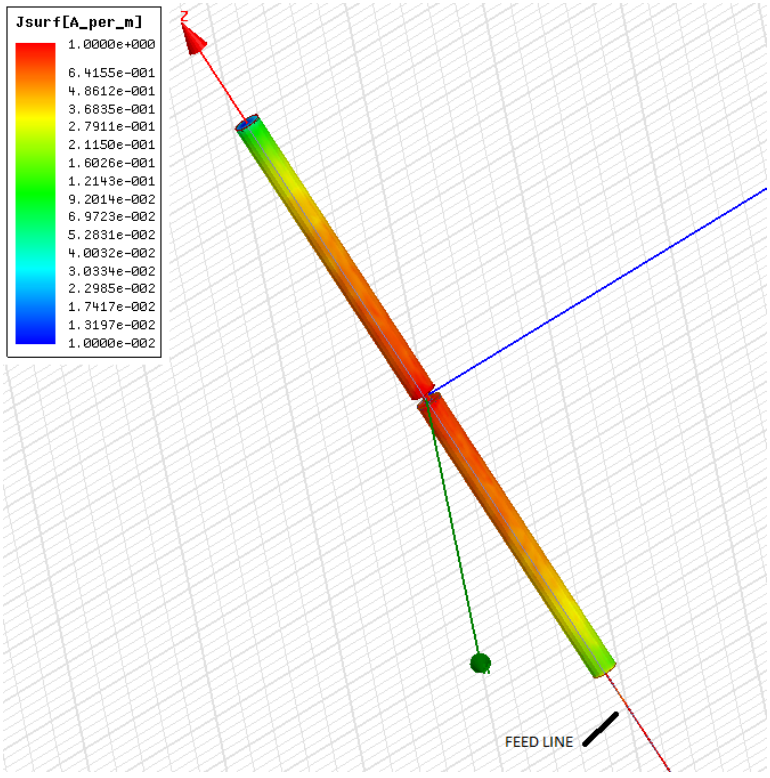

Figure 3.7: Dipole Feed Line Currents without a Choke or Absorber

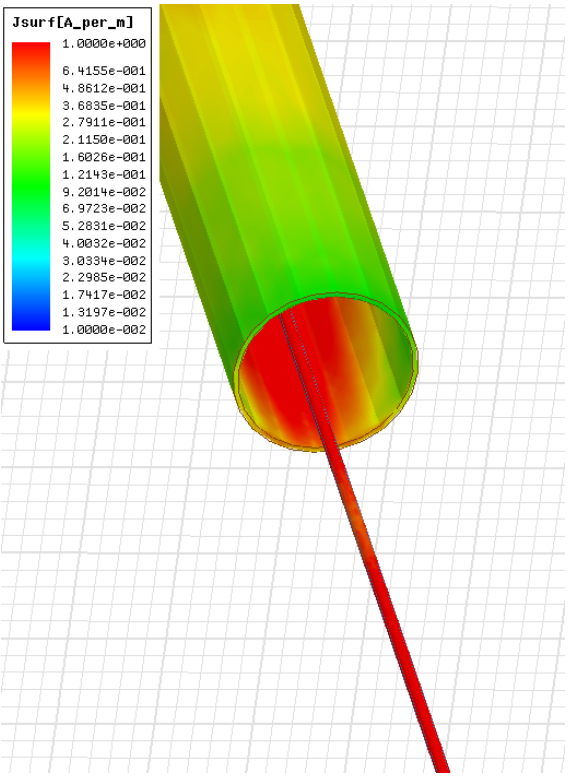

Figure 3.8: Bottom Radiator Feed Line Currents Showing Large Surface Currents Along Feed Line

A choke or absorber prevents antenna performance degradation by limiting the currents from propagating onto the coaxial feed line as shown by plotting the resulting current along the length of the antenna.

3.3 Dipole Antenna Design

Both absorber and resonant choke designs are used in literature. In the dipole antenna design process, the absorber and resonant choke are both analyzed individually and compared. Since the absorber is known to absorb EM energy over a wider frequency band, it does not require much tuning. It can be simply added onto the feed line network and the dipole can be tuned by adjusting the gap spacing for a selected radiator radius and length.

3.3.1 Absorber

A FEM model of the absorber dipole antenna is created to compare the approximate performance with the resonant choke dipole antenna. It should be noted that HFSS can only model nonlinear materials accurately if all the electromagnetic material properties are known. Since there are large variabilities to the doping of ferrite materials, simulation accuracy is limited.

The performance seen in the lab is expected to be significantly different than what is computed by HFSS. Nevertheless, HFSS is still used to compute approximate performance for comparison purposes. An open ended dipole antenna is simulated with a cylindrical ferrite material added to a section of the feed line.

The volumetric currents in the material are clearly dissipated as shown in figure 3.9. It is expected that as currents travel farther from the dipole that they tend to zero. Naturally if the cylindrical material is made larger, the absorbing effects are higher, which may also allow for shorter absorbers.

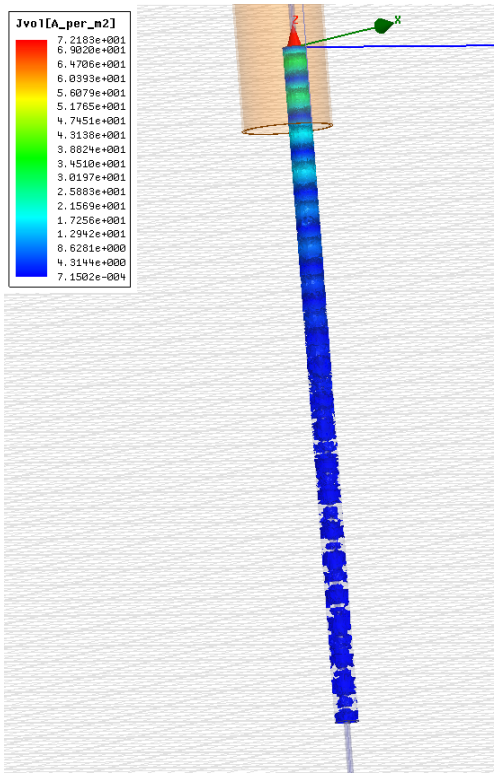

Figure 3.9: Volumetric Current, $|\vec{J}|$, in the Absorber

Using HFSS' calculator feature [4], $|\vec{J}_z|$ is computed along the radiator with the results presented in figure 3.9. Plots of the currents along the length of the antenna with and without the absorber material indicates a significant reduction with the additional material as shown in figure 3.10.

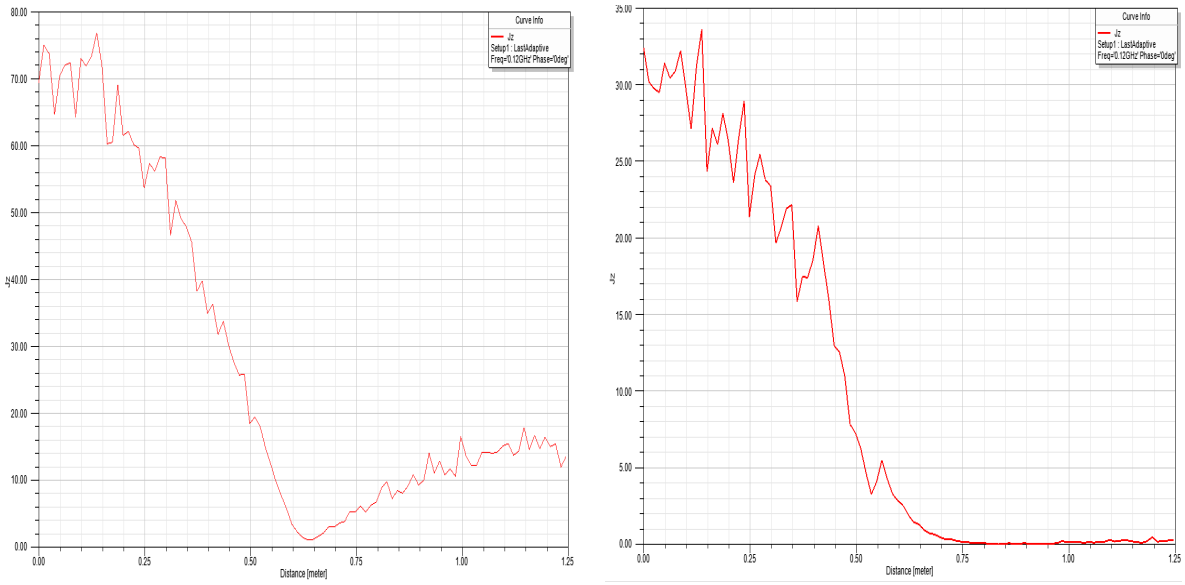

Figure 3.10: Radiator Current Distribution (left: No Absorber right: Absorber Installed)

Currents that propagate down the feed line can radiate into free space, which significantly affects the far field patterns of the antenna. As a direct result of the current distribution along the feed line, the directivity is severely altered as shown on the left side of figure 3.11. Once the absorber is installed, the dipole currents are significantly reduced at the dipole end and the far field performance is regained as shown on the right side of figure 3.11.

The absorber is a simplified means of correcting unwanted currents around the radiator ends for wideband applications. It is seen, however, that the currents along of the feed line are larger and cannot necessarily be tuned at any given frequency. The advantage to a choke model is that the antenna is tuned for the operating frequency band while simultaneously providing a current-free distribution along the feed cable.

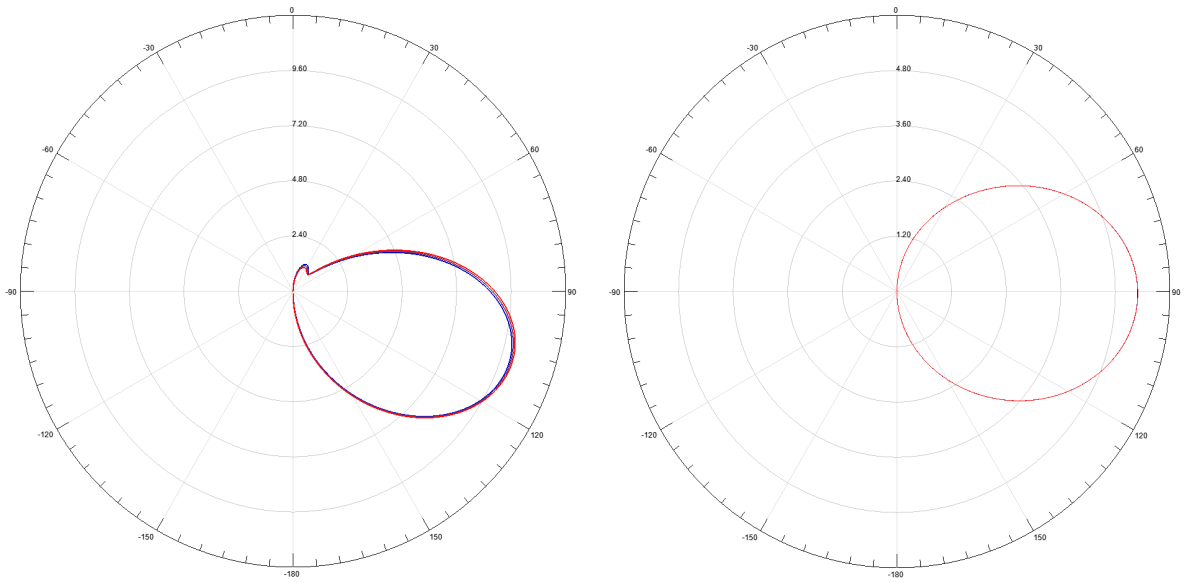

Figure 3.11: Radiator Current Distribution (left: No Absorber right: Absorber Installed)

3.3.2 Choke

The choke solution uses a resonant structure as described in chapter 2 and shown in figure 1.3 to reduce currents along the feed line and reshape the fields to maintain an omnidirectional far field pattern. Internally, currents along the dipole arms continue into the resonant choke, which allows the creation of an effective inductance at the boundary as discussed in chapter 2. This works especially well when the coaxial choke is tuned along with the dipole arms as one unit. To be sure this happens, the characteristic impedance of the choke boundary is designed to match the radiation impedance of the antenna. To match the VHF antenna tuned to 125MHz, the optimal design was found to be at 68.2Ω. The capacitive step is kept as large as possible using the support pipe as the inner conductor.

Using the choke, antenna support, and dipole arm geometry, both the MoM and FEM simulation models are constructed in the matlab code and HFSS respectively. Similarly to the MoM model, line currents computed in the HFSS model are computed along the edge of the antenna radiator as given in figure 3.12.

Since this device does not rely on non-linear materials to absorb currents near the dipole ends, the results should be similar to those found in a center fed case. The currents are computed along the radiator for both the standard finite radius center fed model and

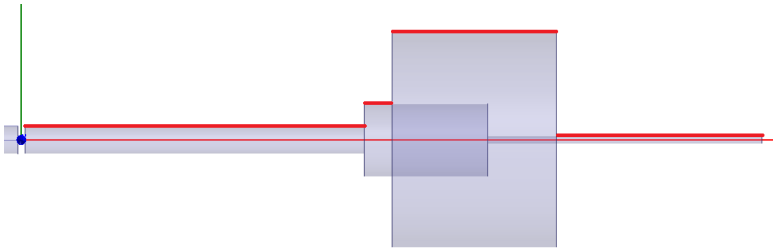

Figure 3.12: Current Computation Along the Radiator

the coaxial feed line finite radius model. The results are computed and compared in figure 3.13. The currents over extend onto the outer choke geometry, which add to the overall effective length of the dipole antenna.

To correct the increased electrical size of the resonant choke antenna, the arm radius and gap distance is kept the same while the ideal center fed arm length is corrected by 0.5in to recenter the resonance to that of the choke model. This allows for an easy comparison of bandwidth changes relative to the same center frequency. It is also noted that the standard dipole current does not go to zero at the ends. This is also seen in the FEM models given in figure 3.3 above. Even though the effective radiator length is extended slightly, the choke acts as a method to smoothly transition edge currents to zero, improving performance for the finite radius model.

The results for VSWR and directivity comparing both the standard textbook dipole and the resonant choke solution is given in figure 3.14. While the standard dipole has the same gap distance and radius at the resonant choke model, the standard dipole arm length corrected so that it is centered at the same center frequency.

The directivity at center frequency is also computed and compared to the standard center fed model. A close correlation between the two models is found. This is expected since the currents along the radiator are significantly attenuated due to the input impedance of the choke structure. Results are shown in figure 3.15.

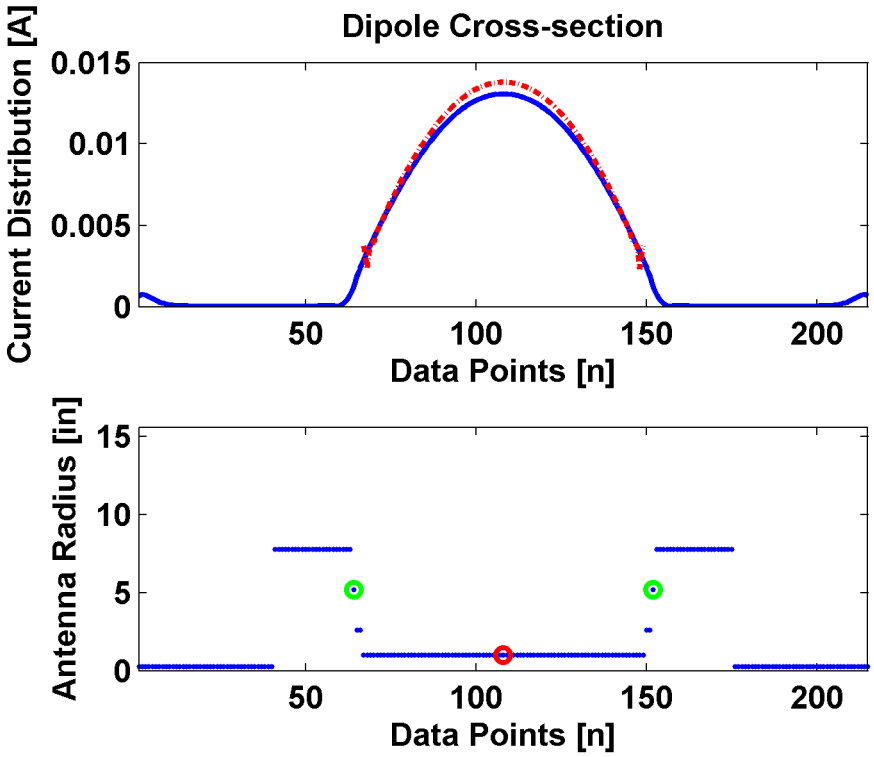

Figure 3.13: Current Distribution Along the Radiator Comparison

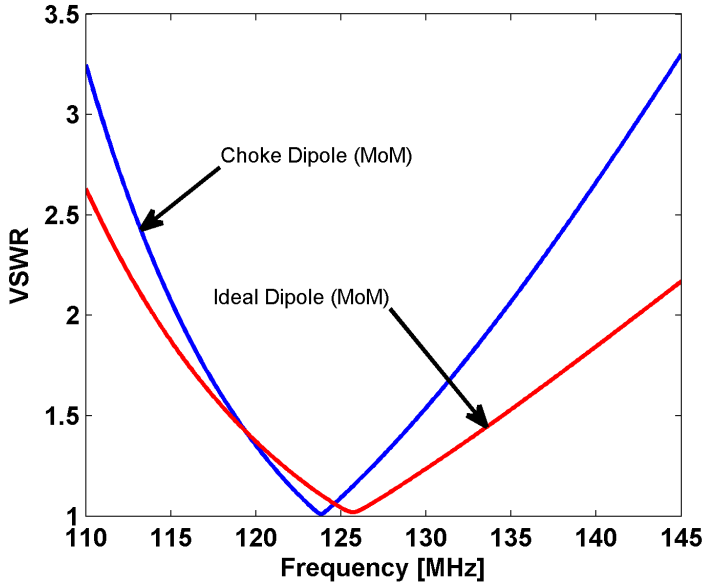

Figure 3.14: VSWR and Directivity Over Frequency Comparison

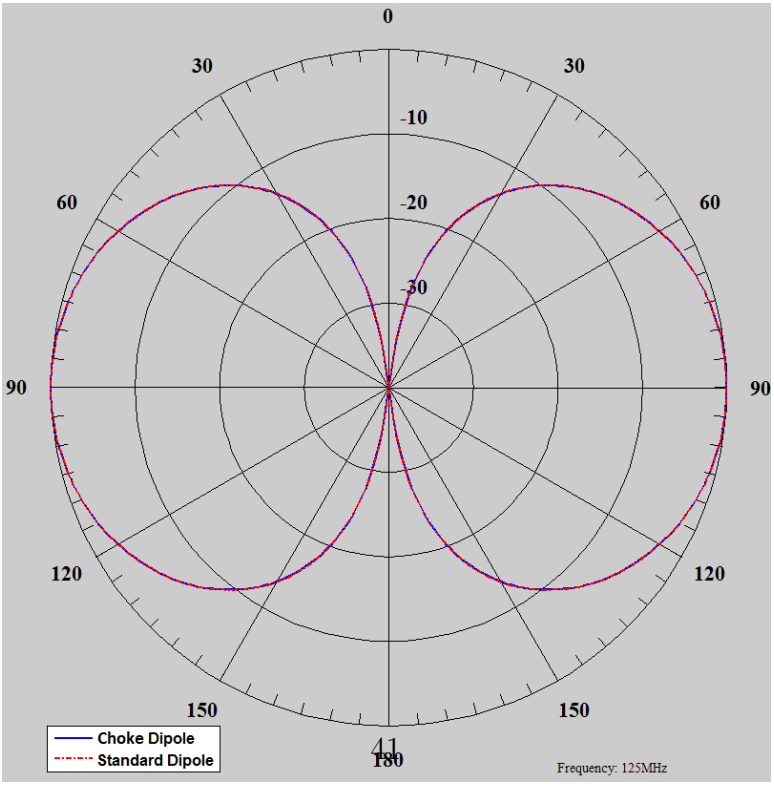

Figure 3.15: Directivity at Center Frequency Comparison

Next, the VSWR and directivity results in the FEM simulation is shown in figures 3.16 and 3.17 respectively. They can be also be compared to the ideal values found in figure 3.6.

3.3.3 Choke vs Absorber

The FEM model of the choke and absorber is now compared. Using HFSS' calculator feature, the radiator line current is computed along the support pipe containing the feed coaxial cable. Comparing the low field sections of each prototype simulation model, the figures 3.18 and 3.19 is produced for the resonant choke and absorber antennas respectively.

It is observed that choke model currents are significantly lower near the bottom of the support pipe at center frequency. Since the choke and dipole are both band limited, they work well when tuned together to a small operating band. Tuning the choke antenna is simple since the effective electrical length of the dipole increases when the choke outer coaxial conductor is positioned further away from the antenna midpoint. This is considered as a tunable feature along with the gap spacing at the source, which is easily implemented in a prototype model.

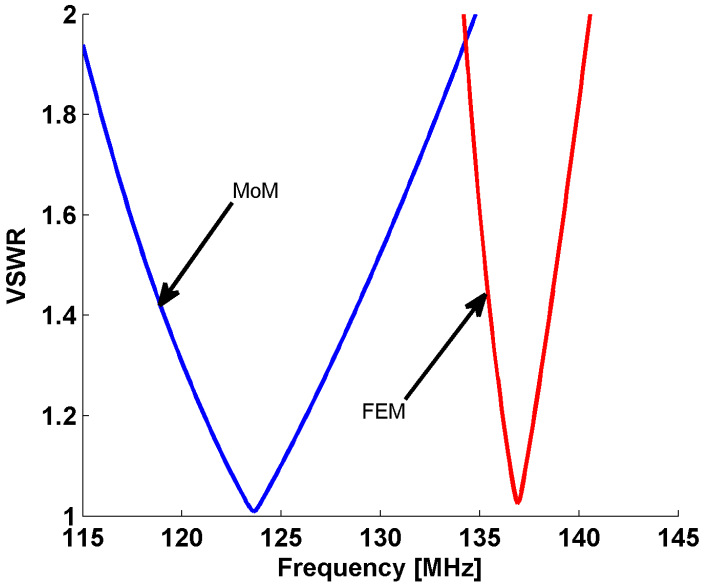

Figure 3.16: Choke Model VSWR Comparison

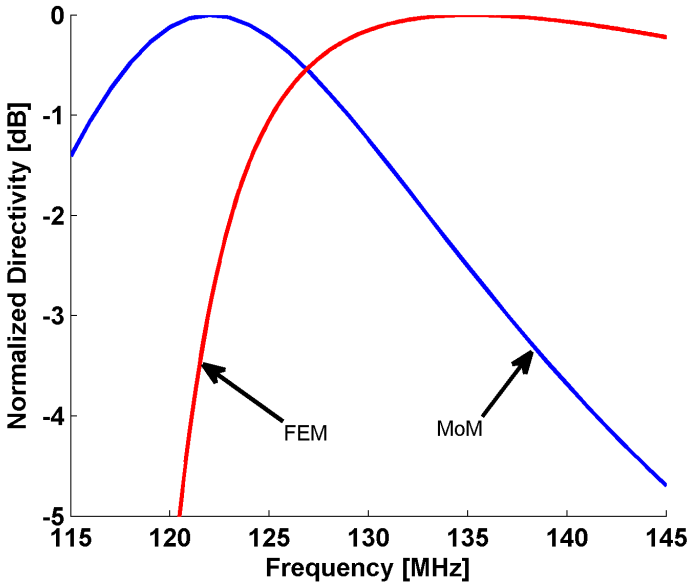

Figure 3.17: Choke Model Directivity Comparison

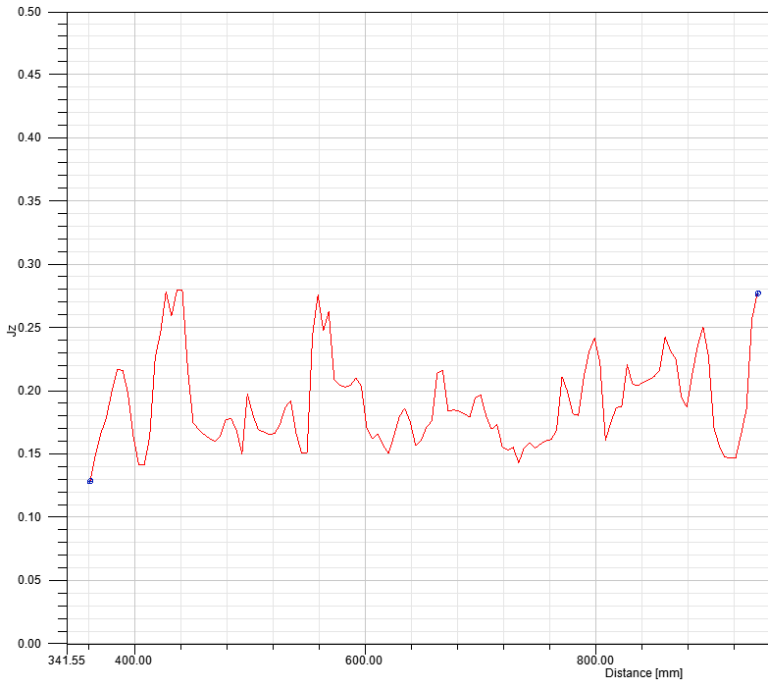

Figure 3.18: Choke: Current Along The Support Pipe

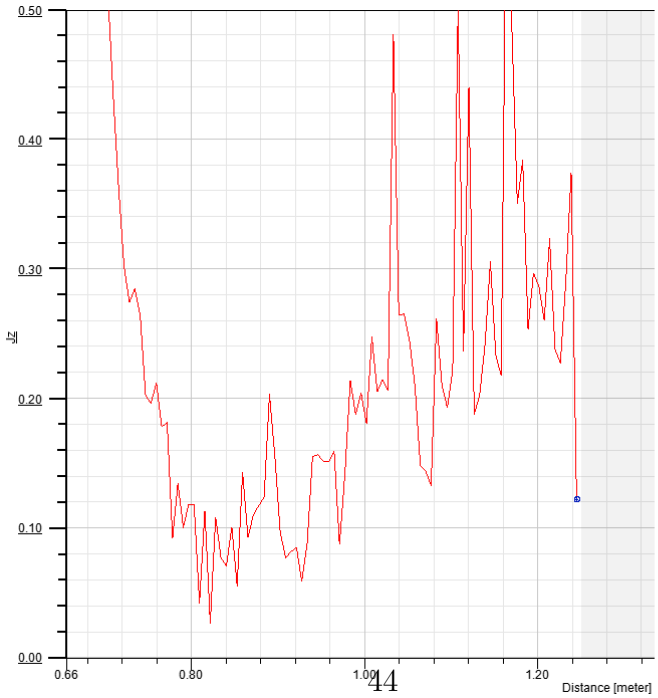

Figure 3.19: Absorber: Current Along The Support Pipe

There are many advantages and disadvantages to both the choke and absorber dipole antennas. While the choke provides excellent dipole performance over a limited bandwidth, the structure itself is larger than the arm radius. Therefore, a radome covering the antenna could be heavy and costly.

Absorber models can offer slightly easier tunability since they only require adjustment of the center gap for a fixed arm length and gap; however, their range is limited. The choke allows for a larger range of tunability using the position of the choke along with the gap to add flexibility to the location of the antenna's center frequency. This is at the expense of using non-linear electromagnetic absorbing materials.

3.4 Feed Network Design

The feed network is designed to allow the dipole to operate efficiently in the required frequency band. As discussed in chapter 2 and shown in figure 2.11, the feed network consists of a 50Ω coaxial cable, a matching balun, and a tuning element. The tuning element is designed using the measured results of the antenna and is discussed in chapter 4.

3.4.1 Balun Design

To design the antenna balun, all other radiative elements were removed and only the balun coax structure was kept. A probe was designed to protrude perpendicular from the coax center conductor to align probe currents with the coax electric field vectors [13]. As the dipole is simulated using a 75Ω input impedance, the output of the balun is designed to match the impedance. The bottom of the balun is shorted to remove the possibility of adding leakage currents back onto the feed line. The enclosed balun structure is given in figure 3.20.

This allows for an excellent transition from the 50Ω feed line to radiator with well matched results shown in figure 3.21. With the available materials, the actual dimensions of the coax become: $R_{SupportPipe} = 0.5in$ OD, $R_{Radiator} = 0.8875in$ ID. A theoretical impedance of 71Ω with a quarter wavelength of 23.2in in the balun section is produced, which is close to the free-space quarter wavelength at 125MHz of 23.6in.

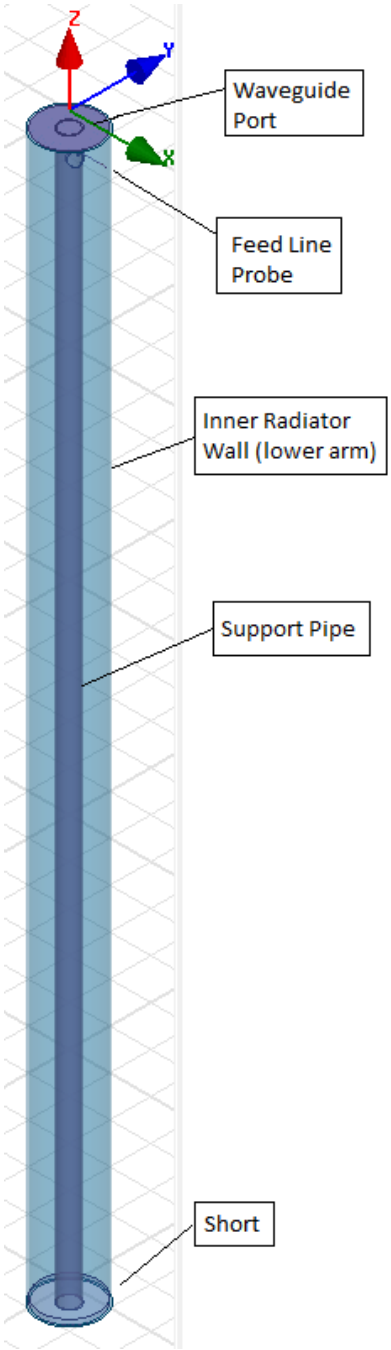

Figure 3.20: Balun: Enclosed HFSS Simulation with Radiator Component Removed

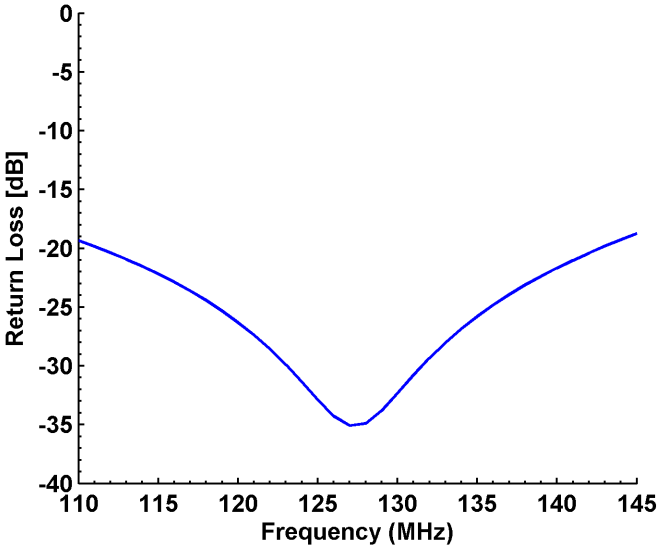

Figure 3.21: Balun: Return Loss

Chapter 4

Antenna Assembly and Measurement

A prototype of the choke and absorber versions of the dipole antenna were manufactured and assembled. A general design is used so that it can accommodate both the resonant choke and absorber dipole antenna types. Both units use the same base antenna specifically designed for ease of manufacturing and assembly. The versatility of the prototype can be seen the figure 4.1.

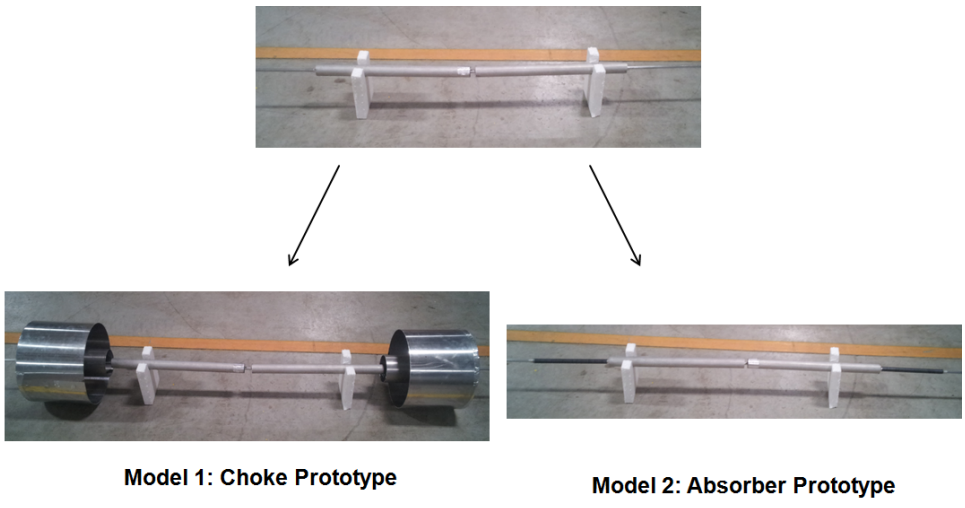

Figure 4.1: DFM Applied to Both Prototypes

The current choking structure was also simplified for ease of tuning on the bench. The internal radius cavity is hollowed due to its evanescent properties and low field strength inside. This allows for easy movement on the bench for testing and tuning. A detailed drawing of the choke is given in figure 4.3.

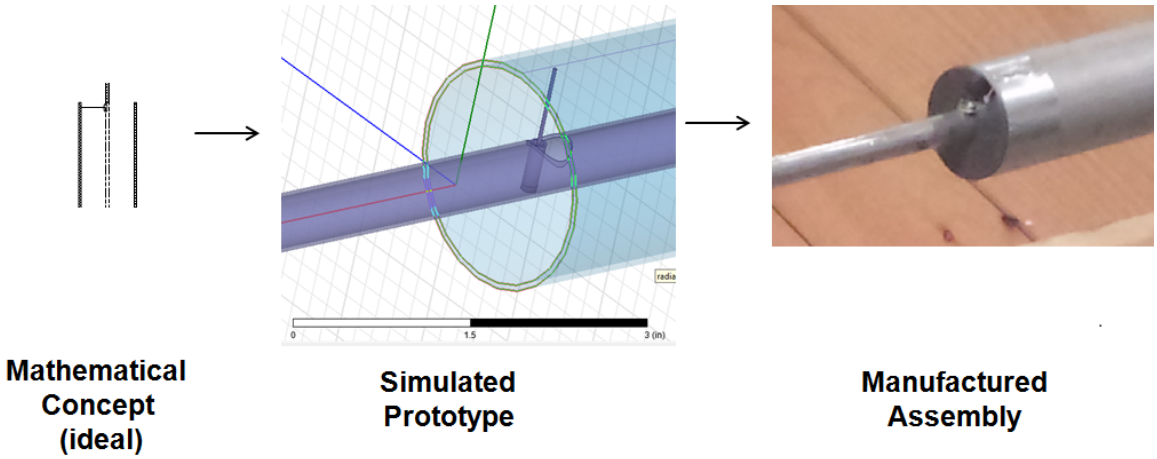

Figure 4.2: Manufactured Transition

Since the source is very sensitive to tuning, the prototype assembly was carefully designed to model the simulation as closely as possible. Figure 4.2 shows how it is taken from its block diagram model, to its manufactured prototype.

Only the choke model was tested for VSWR and relative gain measurements with both dipole antennas mounted parallel to one another. The results are provided in the next section.

4.1 Prototype Antenna

The choke prototype was manufactured, assembled, and tested indoors at the WADE Antenna facility. The WADE Antenna Dipole model D5072 is used as a reference antenna to test the prototype. Since the antenna is an uncalibrated reference antenna, additional tests are recommended. Despite this fact, it is used to measure directivity with respect to frequency and VSWR. A performance gain was achieved for small design bandwidths as shown in figure 4.4.

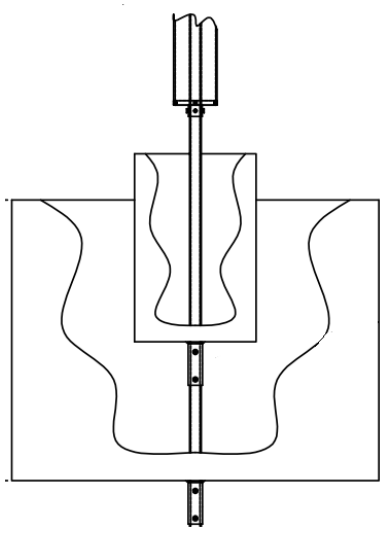

Figure 4.3: Resonant Choke Manufactured Prototype Structure

The as-built fully integrated HFSS model was constructed to compare tuned measured results. The HFSS model is given in figure 4.5, which includes the choke structure, the support structure containing feed cables, and the matching balun. It is observed that an arm length of 25in and a gap size of 2in for a center frequency of 125MHz reported by HFSS was too large. The method of moments code reports an arm length of approximately 20in with a gap size of .5in. To correct for the detuned performance, figure 3.4 is used to increase the center frequency by increasing the source gap distance. By correcting using larger gap sizes and repositioning the choke structure, the following results were achieved with comparison between measured and simulated results in figure 4.6.

4.1.1 Additional Matching Section

As mentioned in Chapter 3, the matching section of this antenna is designed after initial antenna measurements are made. For an accurate antenna matching transformer, single port touchstone file (S1P) is generated as close to the center of the AUT as possible and inserted to into the circuit as shown in figure 4.7 [42].

The circuit is then run through the optimizer to find the optimal lengths of D and L shown in the figure. The distance from the end of the cable to the center feed of the AUT was measured and added to the final length of D. Also, the exact cable characteristics

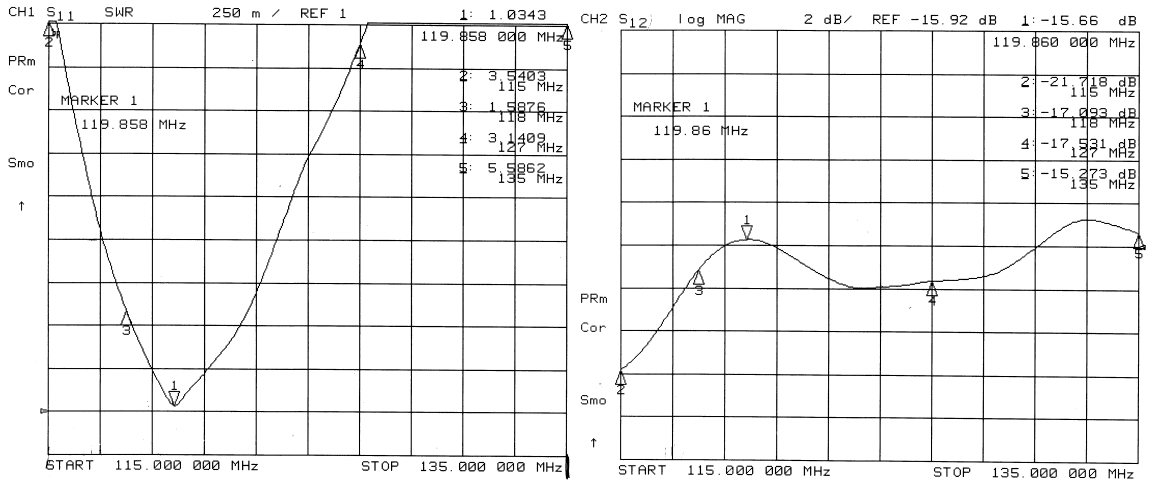

Figure 4.4: First Choke Prototype Measurements

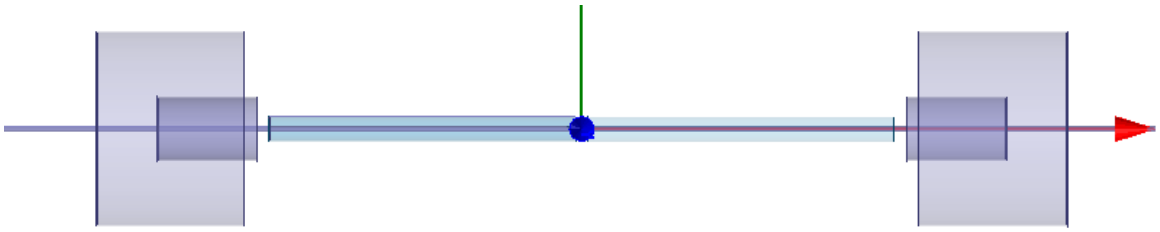

Figure 4.5: HFSS As-built Model Including the Feed Network

were used in the simulator to represent the SM141 feed line coaxial cable as accurately as possible.

The final computed lengths were found to be D=21.2in, and L=21.7in and the results from the simulator are shown in figure 4.8. These results of the simulated antenna assembly correlate with those found by measurement with the new tuning element.

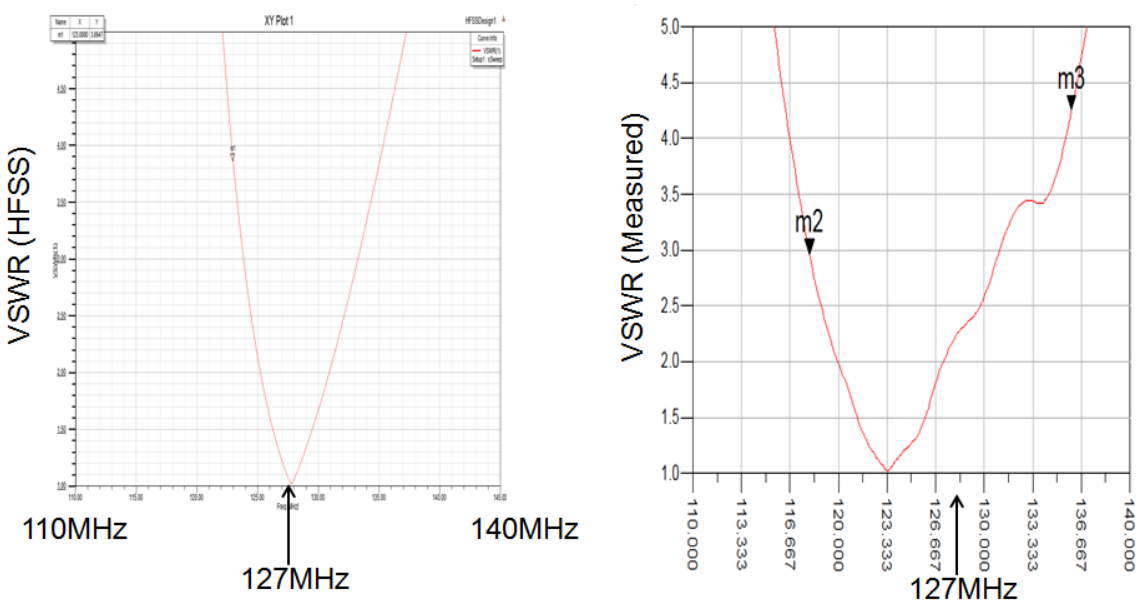

Figure 4.6: VSWR Comparison of the HFSS Simulation vs Measurement

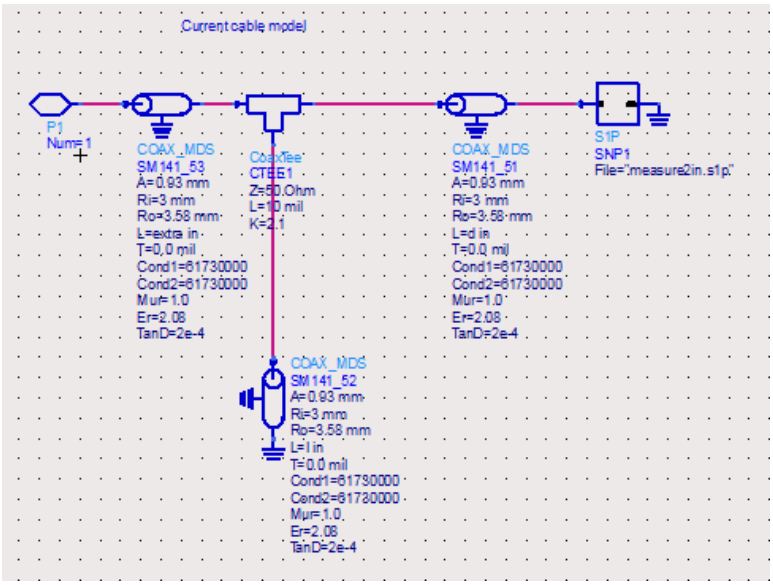

Figure 4.7: ADS Antenna Stub Matching Circuit

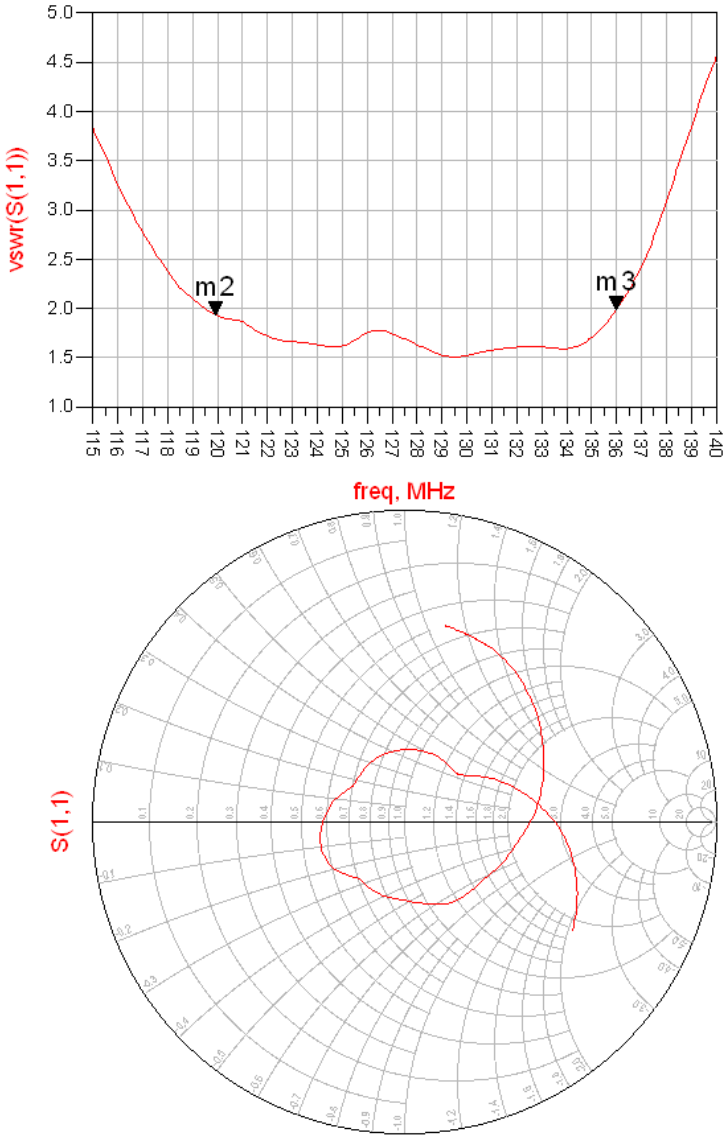

Figure 4.8: ADS Antenna Stub Matching Results

4.2 Test Repeatability and Sources of Error

Although numerical error can be significant for resonant devices, one of the significant sources of measurement error for VHF band dipole antennas are the manufacturing tolerances, assembly errors, and the test setup.

4.2.1 Test Repeatability and Measurement Error

It is clear with the above results that one of the most important factors when measuring any microwave device or radiator is test repeatability. With an uncontrolled test site such as a warehouse, it is difficult to maintain repeatable results. Resonant structures are also prone to detuning from manufacturing and assembly errors. This is especially true for omnidirectional antennas.

Due to the dipole's natural omnidirectional gain pattern, all space around the antenna that is not coated with absorbing materials must be taken into consideration during tests (i.e.: ground, bench, walls, people, etc.). Constructive or destructive reflections returning on to the antenna will appear to increase or decrease performance respectively. This is generally frequency dependent and will look like small or large ripples in the results depending on the scatterer. In either case, this reduces test repeatability and will produce erroneous results.

For an electrically large antenna such as the VHF dipole, a physically large outdoor test setup is recommended to remove most significant scatters. It, however, can be time consuming for tuning this type of antenna. Indoor sites offer the most convenient solution, but also can be error prone with unpredictable scatterers. Testing in a well controlled environment, such as using ferrite beds or electromagnetic absorbing cones surrounding the antenna to prevent radiation reflection, produces the most repeatable results.

Chapter 5

Conclusion Summary, Lessons Learned, and Future Research

The purpose of this project was to determine the source of the dipole's feed line currents and to reduce those currents with prototypeable design. Through the use of many design tools, the current distributions, performance characteristics, and antenna properties were determined. The method of moments provided accurate results while reducing simulation time to a fraction of that used by its finite element method equivalent model. Overall, the process allows for an understanding of the dipole antenna model using both a resonant choking structure and absorbing materials along the coaxial feed line.

Once the antenna model was well understood, a manufacturable prototype was considered to implement both design methodologies. Using Design for Manufacturing, a base prototype was designed to implement the current choke dipole model, but also could support additional research and test on an absorber model.

Finally, the resonant choke model was tested in the lab with results close to that of simulation for VSWR; however, mixed results were obtained for gain. Gain results proved that the many scatterers in the lab changed the performance in unexpected ways in higher frequencies.

5.1 Lessons Learned

Several lessons were learned during the course of this project. These are summarized below.

- The antenna design problem was easily managed by dividing the radiator, choke, balun, and tuning section into separate design stages. This sped up overall antenna design and allowed focus on electrically sensitive areas.
- To accurately model antenna performance, source modelling must be thorough and may require higher order modes such as the coaxial TE_{11} to add accuracy to the current magnetic frill model.
- HFSS simulation model produced resonant frequencies higher than expected by measurement while the MoM produced results that were lower than expected. This is partially due to the resonant nature of the choke structure, which produces varied effective inductance at the enclosed interface boundary.
- Current coupling effects appear to be frequency sensitive and require multiple features to fully support wideband operation due to the choke's resonant nature. Additional research to allow multiple layers inside the choke could help widen bandwidth, but could have a negative effect on high power handling due to the required small gap sizes for coupling between resonators.
- More research is required in absorber materials to use them in an optimized design. Further research was not conducted during this thesis due to the lack of electromagnetic properties for available materials and due to time constraints.

5.2 Future Research Possibilities

Future research possibilities on this project are possible in several areas of research. These are itemized below.

- Mode matching can be used to accurately model internal resonant choke structure as well as the the feed network. This could extend the design parameters to allow better flexibility and design accuracy.
- More tests required for full gain profile and more accurate test results using an outdoor test side or chamber. Together with additional tests and simulation, improvements can be made to the existing prototype to reduce size and complexity.
- A better simulation model for non-linear materials is also required to prevent unexpected test results. This could help reduce the effects of PIM and be a strong competitor to the resonant choke model in terms of overall antenna size. The MoM code could be used as a starting point to implement such a model.
- Additional efforts to construct a more compact resonant choke design could help fit the antenna into more traditional radomes. This could also assist with the structural support of the stacked model.
- Design focus using multilayer chokes with better tuning methods could increase wideband performance. Literature and simulation suggests that increasing the choke complexity could increase the number of resonances and lead to a stackable wideband design.

5.3 Conclusion Summary

The research goal to understand, design, manufacture, assemble, test, and tune a new type of dipole antenna that eliminates currents when configured with a feed coax cable entering either end has been successfully achieved. Simulation and measurements produces correlating results that led to a working design. The resonant choke not only proves to reduce currents lower than other models, but also removes the requirement for non-linear materials to be attached to the antenna. The new type of dipole model including the feed network shows that it can produce results quite close to those generated by the dipole's theoretical center fed counterpart. For these reasons, the resonant choke dipole antenna is a top contender for single or stacked operation.

Appendices

Appendix A

Computer Codes

A.1 Method of Moments in Matlab

Matlab or Octave numerical software can be used with the following code to compute the resonant choke dipole antenna parameters such as VSWR, directivity, gain over frequency, and radiator currents.

A.1.1 Dipole System

Main entry point of the MoM code is given in this first section.

```
% File:  dipoleSystem.m
% Purpose: Computes overall antenna system parameters
% Usage:  dipoleSystem()
% Input:  Program main extry point
% Author:  Steven Petten (c) 2014

function dipoleSystem()

close all;
clear all;
global freq;
global plotideal;
```

```
% Global Variables
plotideal=1; % plots the simple dipole with finite radius in red
% freq        = [115:0.1:135]*1e6; % [Hz] | uncomment to plot RL and gain vs freq
freq        = 125e6;  % [Hz] | uncomment to plot antenna cross section, radiator curren
unit        = units(); % all constants and units
lambda  = unit.c./freq; % wavelength

% Design Parameters | Dimensions for lower half of antenna
Z0          = 75;  % input coax impedance for magnetic frill generator (matching balun
ant.src_gap = in2m(.25);            % 1/2 source gap | best choice based on ideal dipol
ant.arm_l   = in2m(20);             % arm length | resonance sensitive
ant.arm_r   = in2m(0.9375);         % arm radius | specified by available materials
ant.ext_l   = in2m(2);              % resonance sensitive
ant.ext_r   = in2m(2.625);          % insensitive
ant.feed_l  = in2m(30);             % insensitive
ant.feed_r  = in2m(7.8);            % resonance sensitive
ant.src_a   = ant.arm_r;            % resonance sensitive
ant.src_b   = coaxBm(Z0,ant.src_a,1); % port matching impedance
ant.coax_l  = in2m(20);             % insensitive for large values
ant.coax_r  = in2m(.25);            % insensitive
ant.ideal_correction = in2m(.5);    % correction for electrically added length due to t

% Resonant choke input impedance | Zin for Zcb in the MoM code
choke.b1 = ant.feed_r;              % outer wall rad
choke.a1 = ant.ext_r;               % 1st inner wall rad
choke.l1 = in2m(7.125);             % 1st inner wall len
choke.a2 = ant.coax_r;              % 2nd inner wall rad
choke.l2 = ant.feed_l-choke.l1;     % 2nd inner wall len

% Define all geometry in terms of wavelengths
ant.arm_N = round(ant.arm_l/ant.src_gap);  % Determine correct src gap spacing in wavel
if mod(ant.arm_N,2) == 0
     ant.arm_N=ant.arm_N+1;                % if even, add 1
end
ant.ext_N = round((ant.arm_N/(ant.arm_l))*ant.ext_l); % proportional extension segments
if mod(ant.ext_N,2) == 1
     ant.ext_N=ant.ext_N+1;                % if odd, add 1
```

```
end
ant.feed_N = round((ant.arm_N/(ant.arm_l))*ant.feed_l); % proportional choke segments w
if mod(ant.feed_N,2) == 1
     ant.feed_N=ant.feed_N+1;              % if odd, add 1
end
ant.coax_N = round((ant.arm_N/(ant.arm_l))*ant.coax_l); % proportional feed segments w
if mod(ant.coax_N,2) == 1
     ant.coax_N=ant.coax_N+1;              % if odd, add 1
end

% Compute equivalent ideal dipole parameters with the correction factor
idlant=ant;
idlant.arm_l   = ant.arm_l+ant.ideal_correction;  % [m] equivalent resonant ideal dipol
idlant.arm_N = round(idlant.arm_l/idlant.src_gap); % determine correct src gap spacing
if mod(idlant.arm_N,2) == 0
     idlant.arm_N=idlant.arm_N+1;                % if even, add 1
end

% Array storage
[~,szfreq] = size(freq);
zin1 = zeros(1,szfreq);
gain1 = zeros(1,szfreq);
zin2 = zeros(1,szfreq);
gain2 = zeros(1,szfreq);
antvswr1  = zeros(1,szfreq);
antvswr2  = zeros(1,szfreq);
Sp.S11 = zeros(1,szfreq);
Sp.freq  = freq';

for kk=1:szfreq % Loop thru all frequency points
   waitbar(kk/szfreq);% computation status

choke=chokezin(freq(kk),choke);        % compute zin of the resonant choke TL structure
    [zin1(kk),directivity1(kk),plts]=dipoleMOM(ant,lambda(kk),choke.zin(kk)); % choke c
    Sp.S11(kk)=z2gamma(zin1(kk),Z0);
    antvswr1(kk)=gamma2vswr(z2gamma(zin1(kk),Z0)); % compute VSWR
end
```

A.1.2 Diplole MoM

Core MoM code to compute currents along the radiator. This code is also used to compute Zin of the antenna and the directivity [7].

```
% File:  dipoleMOM.m
% Purpose: Computes the method of moments for the axisymmetric
% resonant choke dipole antenna
% Usage:  [zin,directivity,ant] = dipoleMOM(ant,lambda,Zcb)
% Inputs: ant  - antenna geometry in terms of wavelength
% lambda  - wavelength of current solution
% Zcb - Zin of the resonant choke structure
% Ouputs: zin - Zin of the antenna at the source point
% directivity - directivity at theta=90deg
% ant - output geometry and computed values
% Author:  Steven Petten (c) 2014
% Ref:      Balanis, Antenna Theory

function [zin,directivity,ant] = dipoleMOM(ant,lambda,Zcb)

% variables for J1 | Antenna Arms
al=ant.arm_l/lambda; % length of dipole arms (in wavelengths)
ar=ant.arm_r/lambda; % dipole arm radius (in wavelengths)
an=ant.arm_N;
% variables for J2 | Extension
el=ant.ext_l/lambda; % length of dipole extension (in wavelengths)
er=ant.ext_r/lambda; % extention radius (in wavelengths)
en=ant.ext_N;
% variables for J3 | Choke
fl=ant.feed_l/lambda; % length of dipole outer choke (in wavelengths)
fr=ant.feed_r/lambda; % choke radius (in wavelengths)
fn=ant.feed_N;
% variables for J4 | Coaxial Feed Line
cl=ant.coax_l/lambda; % length of dipole coax feed line (in wavelengths)
cr=ant.coax_r/lambda; % feed radius (in wavelengths)
cn=ant.coax_N;

% J1+J2+J3+4
```

```
discons=6;  % count from each end of the discon
ns=(an+en+fn+cn-discons);  % total number of segments
tl=al+el+fl+cl;  % total antenna length=arm+ext+feed+coax
d1 = (cn-1)/2-1+(fn-1)/2; % J3-J2 discontinuity
d2 = d1-1+(en-1)/2;

% Computed parameters
mid=0.5*(ns+1); % mid-point index, assume odd (source generator value for zin)
dz=2*tl/ns; % size of segments
Es=zeros(1,361);
rad=pi/180;
tpi=2*pi;
eta=120*pi;


%% compute impedance matrix by integrating along the surface of the radiator
for k=1:ns % for all segments - double up integration at discontinuities
    zs=tl-(k-0.5)*dz; % source point
    zs1=zs-dz/2; % source lower limit
    zs2=zs+dz/2; % source upper limit
    z=-tl+dz/2; % field point

    %       J1+J2+J3+J4
    if k<(cn-1)/2
        dr=cr;
    elseif k==(cn-1)/2 % coax-J3 discontinuity
        dr=mean([cr,fr]);
    elseif k<d1 % J3 section
        dr=fr;
    elseif k==d1 % J3-J2 discontinuity
        dr=mean([fr,er]);
    elseif k<d2 % J2 section
        dr=er;
    elseif k==d2 % J1-J2 - ceil(ant.ext_N) is the discontinuity point!
        dr=mean([er,ar]);
    elseif k<mid % J1 section, -1 to land on discontinuity point, -1 for source point
        dr=ar;
    elseif k==mid % source gap
```

```
        dr=ar; % TEM Coaxial reference
    elseif k>mid % xy-plane symmetry
        dr=ddr(mid-(k-mid));
    end
    ddr(k)=dr;


    %      Zk integral for lambda<<a
    F = @(zn)exp(-1i*2*pi.*sqrt((z-zn).^2+dr^2)).*((1+1i*2*pi*sqrt((z-zn).^2+dr^2)) ...
        .*(2.*sqrt((z-zn).^2+dr.^2).^2-3*dr*dr) ...
        +(2*pi*dr.*sqrt((z-zn).^2+dr^2)).^2)./(4*pi*sqrt((z-zn).^2+dr^2).^5);

    if(k~=d1) % J3-J2 discontinuity
       Zmn1d(k) = quad(F,zs1,zs2); % use simpson's integration method
    else
       Zmn1d(k) = Zcb; % Resonant choke input impedance
    end
    shape(k) = m2in(dr*lambda); % store the current segment radius
end

% Reorder Zk to compute Zmn
Zmn1d = fliplr(Zmn1d);
for m=1:ns
    for n=1:ns
        Zmn(m,n)=Zmn1d(abs(m-n)+1); % reorder into 2d matrix form
    end
end

%% computes the source field, Ei
a=ant.src_a;
b=ant.src_b;
ba=b/a;
rb=(b/a)*ar;
Vs = 1i*2*pi^2/(eta);
for k=1:ns
    zi=tl-(k-0.5)*dz;
    r1=2*pi*sqrt(zi^2+ar^2);
    r2=2*pi*sqrt(zi^2+rb^2);
```

```
    % far-field magnetic frill excitation without phi dependance
    Ei(k)=-Vs/(2*log(b/a))*(exp(-1i*r1)/r1-exp(-1i*r2)/r2);
end

%% Solve Zmn*I=-Ei for I along radiator
Im=Zmn\(-Ei'); % Es = -Ei
zin=1/Im(mid); % Zin at the center of hte radiator
Es=computeDirectivity(Im);
maxgain=max(Es);
directivity=Es(91);
```

A.1.3 Resonant Choke

This section of code computes Zcb for the internal resonant choke structure.

```
% File:  chokezin.m
% Purpose: Computes Zcb for the internal resonant choke structure for use in MoM
% Usage:  choke = chokezin(freq, choke)
% Author:  Steven Petten (c) 2014

function choke = chokezin(freq, choke)

% compute Zin for the resonant choke
[ABCD1,Z1] = coaxABCD(freq, choke.a1,choke.b1,choke.l1, 1, 1,1e20,0);
[ABCD2,Z2] = coaxABCD(freq, choke.a2,choke.b1,choke.l2, 1, 1,1e20,0);
s2 = a2s(ABCD2,abs(Z2));
Scoax_step = coaxStep(choke.b1,choke.a1,choke.a2,1,freq);
s_choke = cascadesparams(s1,Scoax_step);
s_choke = cascadesparams(s2,s_choke);
s_choke = cascadesparams(s_choke,[-1 0; 0 0]);
zres = computeRes(freq);
choke.zin = s2z(s_choke(1,1),abs(Z1))+zres;
```

A.1.4 Coaxial Step Discontinuity

This code computes the scattering parameters of the coaxial step discontinuity.

```
% File:  coaxStep.m
% Purpose: Computes S-parameters of a coax to coax step discontinuity
% Usage:  S = coaxStep(b1,a1,a2,eps_r,freq)
% Inputs: b1  - coax outer conductor radius
% a1  - coax1 inner conductor radius
% a2 - coax2 inner conductor radius
% eps_r - Coax dielectric permitivity
% freq - Solution frequency
% Ouputs: S - S-parameters of the coax step
% Author:  Steven Petten (c) 2014
% Ref:  Somlo, "The Computation of Coaxial Line Step Capacitances"

function S = coaxStep(b1,a1,a2,eps_r,freq)
unit = units;

% check a2>a1, if not swap
if a1>a2
    t=a1;
    a1=a2;
    a2=t;
end

% Somlo ckt approximation
a = (b1-a2)/(b1-a1); % 0<alpha<1
if (a<0.01 || a>1)
    alpha=a
    error('requirement: 0.01<=alpha<=1, check coax radii');
end
Cd = unit.eps0*eps_r/(pi)*(((a^2+1)/a)*log((1+a)/(1-a))-2*log(4*a/(1-a^2))); %[F/m]

om=2*pi.*freq;
B = 1/(1i.*om.*Cd);
jB = -B/(2+B);
S = [jB 1+jB; 1+jB jB];
```

A.1.5 Lossy Coaxial Line ABCD-parameters

This code computes the ABCD-parameters of a lossy coaxial line [42]. This code can easily be converted to s-parameters [39].

```
% File:  coaxABCD.m
% Purpose: Computes ABCD-parameters of a lossy coaxial waveguide
% Usage:  [ABCD,Z0] = coaxABCD(freq, a,b,len, eps_r, mu_r,sigma_cond,tand)
% Inputs: freq  - Solution frequency
% a  - inner conductor radius
% b - outer conductor radius
% len - length of coax
% eps_r - Coax dielectric permitivity
% mu_r - Coax dielectric permeability
% sigma_cond - conductivity
% tand - loss factor
% Ouputs: ABCD - ABCD-parameters of the lossy coax waveguide
% Author:  Steven Petten (c) 2014
% Ref:  Pozar, Microwave Engineering 3rd ed.

function [ABCD,Z0] = coaxABCD(freq, a,b,len, eps_r, mu_r,sigma_cond,tand)
unit = units;

% skin depth
tand_cond = 1./sqrt(pi*freq*unit.mu0*mu_r*sigma_cond);
% eps = eps' + j*eps''
eps_p = unit.eps0*eps_r;
eps_pp = unit.eps0*eps_r*tand;

L = (unit.mu0*mu_r/(2*pi))*log(b/a);
C = 2*pi*eps_p/log(b/a);
R = (1./(2*pi*sigma_cond*tand_cond))*(1/a+1/b);
G = ((2*pi)^2).*freq.*eps_pp./log(b/a);

[Z0,k] = lcrg2z(freq,L,C,R,G);
[ABCD] = abcd_wg(k*len,Z0);
```

References

[1] *Electromagnetic Waves and Antennas*. Pearson Higher Education & Professional Group, 2003.

[2] Agilent. Advanced design system 2013.06. 2013. [Online]. Available: www.agilent.com.

[3] J. Andersen, Hans Schj\a er Jacobsen, and H. Lessow. Coupling between crossed-dipole feeds. *Antennas and Propagation, IEEE Transactions on*, 22(5):641646, 1974.

[4] Ansys. Fields calculator cookbook-a brief primer and collection of step-by-step calculator recipies for use in hfss fields post-processing. 2012.

[5] Ansys. High frequency structural simulator v15. 2013. [Online]. Available: http://www.ansys.com.

[6] C.A. Balanis. *Advanced Engineering Electromagnetics*. CourseSmart Series. Wiley, 2012.

[7] C.A. Balanis. *Antenna Theory: Analysis and Design*. Wiley, 2012.

[8] T. S. Bird. Exact solution of open-ended coaxial waveguide with centre conductor of infinite extent and applications. In *Microwaves, Antennas and Propagation, IEE Proceedings H*, volume 134, page 443448. IET, 1987.

[9] K.J. Byers, A.R. Harish, S.A. Seguin, C.J. Leuschen, F. Rodriguez-Morales, J. Paden, E.J. Arnold, and R.D. Hale. A modified wideband dipole antenna for an airborne vhf ice-penetrating radar. *Instrumentation and Measurement, IEEE Transactions on*, 61(5):1435–1444, May 2012.

[10] David C. Chang. On the electrically thick monopole: Part ITheoretical solution. *Antennas and Propagation, IEEE Transactions on*, 16(1):5864, 1968.

[11] D.C. Chang. On the electrically thick monopole - part ii - experimental study. *Antennas and Propagation, IEEE Transactions on*, 16(1):64–71, January 1968.

[12] Huang Chang-Hsiu and Powen Hsu. Effect of feed modeling on the evaluation of input impedance of microstrip antennas. *Magnetics, IEEE Transactions on*, 25(4):3058–3060, Jul 1989.

[13] R.E. Collin. *Foundations for Microwave Engineering*. IEEE Press Series on Electromagnetic Wave Theory. Wiley, 2001.

[14] COMSOL. Comsol multiphysics. 2014. [Online]. Available: www.comsol.com.

[15] A. Derneryd, M. Gustafsson, G. Kristensson, and C. Sohl. Application of gain-bandwidth bounds on loaded dipoles. *Microwaves, Antennas Propagation, IET*, 3(6):959–966, September 2009.

[16] S. Egashira, T. Tanaka, and A. Sakitani. A design of am/fm mobile telephone triband antenna. *Antennas and Propagation, IEEE Transactions on*, 42(4):538–540, Apr 1994.

[17] Alan J. Fenn, Peter T. Hurst, James D. Krieger, John S. Sandora, and Leonard I. Parad. Ultrawideband VHF/UHF dipole array antenna. In *Phased Array Systems and Technology (ARRAY), 2010 IEEE International Symposium on*, page 7982. IEEE, 2010.

[18] A. R. Guraliuc, A. A. Serra, P. Nepa, and G. Manara. Parasitic current reduction on electrically long coaxial cables feeding dipoles of a collinear array. *IEEE Transactions on Antennas and Propagation*, 59(11):4318–4321, November 2011.

[19] R.C. Hansen. Efficiency and matching tradeoffs for inductively loaded short antennas. *Communications, IEEE Transactions on*, 23(4):430–435, Apr 1975.

[20] R.F. Harrington. *Field Computation by Moment Methods*. IEEE/OUP Series on Electromagnetic Wave Theory. Oxford University Press, USA, 1993.

[21] C. Icheln, Joonas Krogerus, and P. Vainikainen. Use of balun chokes in small-antenna radiation measurements. *Instrumentation and Measurement, IEEE Transactions on*, 53(2):498–506, April 2004.

[22] C. Icheln, J. Ollikainen, and P. Vainikainen. Reducing the influence of feed cables on small antenna measurements. *Electronics Letters*, 35(15):1212–1214, Jul 1999.

[23] C. Icheln and P. Vainikainen. Dual-frequency balun to decrease influence of rf feed cables in small antenna measurements. *Electronics Letters*, 36(21):1760–1761, Oct 2000.

[24] J.M. Jin. *Theory and Computation of Electromagnetic Fields*. Wiley, 2011.

[25] J. Johnson, R. Rimmer, and J. Corlett. Computer simulations of a wide-bandwidth ferrite-loaded high-power waveguide termination. *Power (Watts)*, 714(1200):1200, 1996.

[26] A. A. Kishk, L. Shafai, and A. Ittipiboon. Improvement in radiation characteristics of coaxial feeds using a quarter-wavelength choke. *Electronics Letters*, 20(12):522523, 1984.

[27] J.D. Kraus. Antennas since hertz and marconi. *Antennas and Propagation, IEEE Transactions on*, 33(2):131–137, February 1985.

[28] K. W. Leung, K. M. Luk, K. Y. A. Lai, and D. Lin. Theory and experiment of a coaxial probe fed hemispherical dielectric resonator antenna. *Antennas and Propagation, IEEE Transactions on*, 41(10):13901398, 1993.

[29] W. R. Lind and R. J. Kalagher. Mode selective coaxial directional couplers for harmonic measurements. *Electromagnetic Compatibility, IEEE Transactions on*, (1):2531, 1966.

[30] L Liu, SW Cheung, YF Weng, and TI Yuk. Cable effects on measuring small planar uwb monopole antennas. *Ultra wideband-current status and future trends, ISBN*, pages 978–953, 2012.

[31] M.D. Lockard and C.M. Butler. Effects of cavities on monopole antenna current distribution and decoupling from mounting structure. *IEEE Transactions on Antennas and Propagation*, 54(8):2234–2243, August 2006.

[32] SURITA Maini and ANUPMA Marwaha. Comparison of coaxial choke and extended tip choke antenna for interstitial microwave ablation of HCC. In *Information and Communication Technologies (WICT), 2011 World Congress on*, page 841845. IEEE, 2011.

[33] N. Marcuvitz and Institution of Electrical Engineers. *Waveguide Handbook*. IEE electromagnetic waves series. P. Peregrinus, 1951.

[34] MathWorks. Matlab r2012a. 2012. [Online]. Available: http://www.mathworks.com.

[35] J. Mclean, M. Leuvano, and Heinrich Foltz. Reduced-size, folded ground plane for use with low-profile, broadband monopole antennas. In *Radio and Wireless Conference, 1999. RAWCON 99. 1999 IEEE*, page 239242. IEEE, 1999.

[36] K. Mei and J. van Bladel. Scattering by perfectly-conducting rectangular cylinders. *Antennas and Propagation, IEEE Transactions on*, 11(2):185–192, Mar 1963.

[37] T.A. Milligan. *Modern Antenna Design*. Wiley, 2005.

[38] T. Ogiwara, T. Hirano, J. Hirokawa, and M. Ando. 2-d mom analysis of the choke structure for isolation improvement between two waveguide slot array antennas. In *Microwave Conference, 2007. APMC 2007. Asia-Pacific*, pages 1–4, Dec 2007.

[39] Sophocles J. Orfanidis. *ElectromagneticWaves and Antennas*. 2014. [Online]. Available: http://www.ece.rutgers.edu/ orfanidi/ewa/.

[40] Maria Pardalopoulou and Klaus Solbach. Over-moded operation of waveguide-to-coax transition at 60 GHz. In *Infrared and Millimeter Waves, 2004 and 12th International Conference on Terahertz Electronics, 2004. Conference Digest of the 2004 Joint 29th International Conference on*, page 475476. IEEE, 2004.

[41] J.C. Pedro and N.B. Carvalho. *Intermodulation Distortion in Microwave and Wireless Circuits*. Artech House microwave library. Artech House, Incorporated, 2002.

[42] D.M. Pozar. *Microwave Engineering*. Wiley, 2011.

[43] S.A. Saario, D.V. Thiel, S.G. O'Keefe, and J.W. Lu. Analysis of ferrite beads for rf isolation on straight wire conductors. *Electronics Letters*, 33(16):1359–1360, Jul 1997.

[44] S.A. Schelkunoff and H.T. Friis. *Antennas: theory and practice*. Applied mathematics series. Wiley, 1952.

[45] Roland Schwerdtfeger. A coaxial dual mode feed system. In *Microwave Conference, 1979. 9th European*, page 196200. IEEE, 1979.

[46] G.R. Simpson. A generalized n-port cascade connection. In *Microwave Symposium Digest, 1981 IEEE MTT-S International*, pages 507–509, June 1981.

[47] P.I. Somlo. The computation of coaxial line step capacitances. *Microwave Theory and Techniques, IEEE Transactions on*, 15(1):48–53, Jan 1967.

[48] N. Stevens and L. Martens. Model of a dipole antenna in free-space and near a perfectly electrical conducting plate. *IEEE Transactions on Antennas and Propagation*, 53(5):1672–1680, May 2005.

[49] M.A. Tilston and K.G. Balmain. A multiradius, reciprocal implementation of the thin-wire moment method. *Antennas and Propagation, IEEE Transactions on*, 38(10):1636–1644, Oct 1990.

[50] W.V. Tilston and A.H. Secord. A 3 kw high gain colinear antenna for v.h.f. multicoupling. *IEEE Transactions on Vehicular Communications*, 12(1):93–107, Sept 1963.

[51] L. Tsai. A numerical solution for the near and far fields of an annular ring of magnetic current. *Antennas and Propagation, IEEE Transactions on*, 20(5):569–576, Sep 1972.

[52] D.H. Werner. A method of moments approach for the efficient and accurate modeling of moderately thick cylindrical wire antennas. *Antennas and Propagation, IEEE Transactions on*, 46(3):373–382, Mar 1998.